https://doi.org/10.5194/egusphere-2024-1941
Preprint. Discussion started: 18 September 2024

Coupled Carbon-Nitrogen Cycle in MAGICC v1.0.0: Model Description and Calibration

Gang Tang[1], Zebedee Nicholls[2], Alexander Norton[3], Sönke Zaehle[4], Malte Meinshausen[1]

[1]School of Geography, Earth and Atmospheric Sciences, The University of Melbourne, Melbourne, Australia
[2]Energy, Climate and Environment (ECE) Program, International Institute for Applied Systems Analysis (IIASA), Laxenburg, Austria
[3]Research School of Biology, Australian National University, Canberra, Australia
[4]Department of Biogeochemical Signals, Max Planck Institute for Biogeochemistry, Jena, Germany

Correspondence to: Gang Tang (gang.tang.au@gmail.com)

Abstract. The integration of a nitrogen cycle represents a recent advancement in Earth System Models (ESMs). However, diverse formulations and representations introduce uncertainties and inconsistencies in nitrogen effects on the carbon cycle, leaving the global carbon-nitrogen coupling effect unclear. In this study, we present the newly developed carbon-nitrogen coupling in MAGICC, a reduced complexity model (RCM). We have calibrated this coupled carbon-nitrogen cycle to two land surface models (CABLE and OCN) and (the land component of) a set of CMIP6 ESMs. The new carbon-nitrogen coupled model is able to capture the dynamics of the more complex models' carbon-nitrogen cycle at the global-mean, annual scale. The emulation results suggest a consistent nitrogen limitation on net primary production (NPP) in CMIP6 ESMs, persisting throughout the simulations (i.e. over the period 1850-2100) in most models. The emulation may provide a way to disentangle diverse nitrogen effects on carbon pool turnovers in CMIP6 ESMs, with our results suggesting that nitrogen deficiency generally inhibits litter production and decomposition while enhancing soil respiration (from a multi-model mean perspective). However, this disentanglement is limited due to a lack of simulations from CMIP6 ESMs which would allow us to cleanly separate the nitrogen and carbon responses. The results imply a potential reduction in land carbon sequestration in the future due to nitrogen deficiency. Future studies will use the newly developed model to further investigate the carbon-nitrogen coupling effect and its associated uncertainty.

1 Introduction

Atmosphere-Ocean General Circulation Models (AOGCMs) and Earth System Models (ESMs) are currently the most powerful tools that integrate our understanding of climate physics and provide comprehensive projections for the global climate and its variability (Meehl, 1990). However, these complex models require large computational power for their simulations while the difference in assumptions, parameterizations and structures, across models often hinders a systematic quantification of uncertainties (Ohgaito et al., 2013). To combine the latest insights from various AOGCMs and ESMs, Simple Climate Models (SCMs) - also called Reduced-Complexity Climate Models (RCMs) - are developed and routinely

https://doi.org/10.5194/egusphere-2024-1941
Preprint. Discussion started: 18 September 2024

updated to represent and integrate the full uncertainty spectrum across the cause-effect chain of climate change (Nicholls et al., 2020; Nicholls et al., 2021). The highly parameterized formulations in RCMs can, in some cases, parameterize the structural uncertainties from complex models. The flexibility of RCM structures also allows for factor separation analysis to disentangle the key processes affecting the climate. With these features, RCMs are widely used for ensemble projections of scenarios and regularly feed into climate policy.

The Model for the Assessment of Greenhouse Gas Induced Climate Change (MAGICC), originally introduced by Wigley and Raper (Wigley and Raper, 1987, 1992, 2001) and further developed since (Meinshausen et al., 2011a; Nauels et al., 2017; Meinshausen et al., 2020), is a key RCM that has been used for scenario classification in multiple IPCC reports (e.g., IPCC, 2014: Climate Change 2014: Synthesis Report, IPCC, 2018: Global Warming of 1.5°C, IPCC, 2023: Climate Change 2023: Synthesis Report). MAGICC's main design principle is this: be as simple as possible while as mechanistic as necessary in the sense of being based on physical principles and/or long-term ESM calibrations (Meinshausen et al., 2011a).

The nitrogen cycle is a critical part in the Earth system's biogeochemistry which has a significant impact on climate alongside other element cycles like carbon, phosphorus, etc. (Fowler et al., 2013; Elser et al., 2007). As an essential nutrient for numerous fundamental biological processes, nitrogen is one of the major factors controlling the terrestrial carbon cycle and thus influences the carbon-concentration and carbon-climate feedbacks (Zaehle et al., 2010; Zaehle and Dalmonech, 2011; Fowler et al., 2013; Zaehle, 2013), the two main carbon cycle feedbacks (Arora et al., 2020). The integration of the nitrogen cycle and its effects within carbon cycle models is a recent advancement in ESMs. Only three CMIP5 ESMs (CCSM, CESM, NorESM), all of which had the same land component (CLM4), included the nitrogen cycle (Flato et al., 2014). However, at least 17 out of 39 CMIP6 ESMs included a nitrogen cycle (see IPCC, 2021: Annex II: Models). Various assumptions and formulations have been incorporated into the nitrogen cycle and the carbon-nitrogen coupling (Meyerholt and Zaehle, 2015; Meyerholt et al., 2020), resulting in divergent responses of the carbon cycle (Zaehle et al., 2015; Davies-Barnard et al., 2020; Arora et al., 2020; Kou-Giesbrecht and Arora, 2022).

Generally, the inclusion of the nitrogen cycle largely reduces land carbon sequestration under increasing atmospheric CO_2 and warming conditions by amplifying both plant respiration (thus limiting NPP) and soil organic matter decomposition (Thornton et al., 2007; Sokolov et al., 2008). On average, the carbon-nitrogen coupled ESMs have smaller carbon-concentration feedback and smaller carbon-climate feedback compared to their carbon-only counterparts (Arora et al. 2020). Plant nitrogen uptake, carbon:nitrogen ratio, nitrogen regulation of photosynthesis, and biological nitrogen fixation contribute to the NPP difference (Du et al., 2018). Carbon-nitrogen interaction simulations from JSBACH have suggested a moderate reduction of the carbon-concentration feedback, while showing a negligible effect on carbon-climate feedback (Goll et al., 2017). However, enhanced soil organic matter decomposition under warming increases mineral nitrogen availability, thereby conversely leading to increased land carbon sequestration on vegetation. The relative strength of these compensating effects remains unclear. Integrating and parameterizing the nitrogen cycle in RCMs is therefore an ongoing research need for better understanding and comparing ESMs.

https://doi.org/10.5194/egusphere-2024-1941
Preprint. Discussion started: 18 September 2024

The significance of the nitrogen cycle highlights the need to capture its effects within a key tool in climate science, namely reduced complexity climate models. To the best of our knowledge, there is currently no RCM featuring the nitrogen effect, let alone a fully coupled carbon-nitrogen cycle. As a result, this study introduces an updated carbon-nitrogen model, intended for use as MAGICC's carbon cycle. Section 2 presents a detailed description of the land carbon-nitrogen cycle and carbon-nitrogen coupling in MAGICC. Section 3 provides offline calibration results for two land surface models and a series of CMIP6 ESMs across multiple scenarios. The related discussions and analysis, primarily focusing on the CMIP6 ESMs, are presented in Section 4. Section 5 discusses the limitations and implications of the coupled carbon-nitrogen cycle model for MAGICC. The updated MAGICC is shown to capture the global aggregate effects of coupling the nitrogen cycle with the carbon cycle when considering the latest generation of specialized domain models and ESMs. In future work, it will be used to explore one of the main uncertainties in future climate projections: the uncertain development of future CO_2 concentrations given the intertwined carbon cycle feedback, CO_2 fertilization, and nitrogen cycle effects.

2 Model description

2.1 Overview of MAGICC

MAGICC is one of the most widely used RCMs, originating from the simple global mean energy balance equation. MAGICC features variable climate sensitivities and a carbon cycle that has successfully emulated a series of CMIP3 AOGCMs and C4MIP carbon cycle models (Meinshausen et al., 2011a). The most recent updates of MAGICC include the introduction of variable climate sensitivities and the updated carbon cycle (Meinshausen et al., 2011a), the incorporation of a sea level model (Nauels et al., 2017) and various improvements over time with regard to radiative forcing schemes etc. (Meinshausen et al., 2020).

The continuously expanding understanding of climate physics, chemistry and biology, coupled with the rapid development of complex models, necessitates the corresponding advancement of RCMs for more accurate emulations. Here we focus on the development of the terrestrial carbon-nitrogen cycle in MAGICC. As a brief background, the initial design of the nitrogen cycle considered nitrogen processes at a similar level of detail as complex models do (albeit at a global scale rather than grid-box scale, e.g., the box model design starts from the major state variables and fluxes that are required by C4MIP) (Jones et al., 2016). However, during model parameterization and refinement, some processes have been eliminated or combined with others to reach a balance between model simplicity and model performance, following MAGICC's overall design philosophy of being as simple as possible, but not simpler.

2.2 The mass balance of carbon and nitrogen in MAGICC

MAGICC's carbon-nitrogen cycle model is a globally integrated and annually averaged box model (Fig. 1). The carbon-nitrogen cycle comprises the carbon pools of 'plant' (P), 'litter' (L), and 'soil' (S), along with their corresponding nitrogen pools, as well as the inorganic 'mineral' (M) nitrogen pool. The pools are interlinked by a system of first-order differential

https://doi.org/10.5194/egusphere-2024-1941
Preprint. Discussion started: 18 September 2024

equations (Eqs. 1-9). The 'atmosphere' (A) exchanges carbon with the land carbon pools via 'net primary production' (NPP), heterotrophic respiration, and 'land use or other anthropogenic fluxes' (LU). The heterotrophic respiration includes 'plant litter production respiration' (LPR, the litter respiration produced from plant litter production that is released back to the atmosphere within a single timestep, typically one year for MAGICC), 'soil respiration' (SR); and 'litter decomposition that directly goes into atmosphere' (LD2A, i.e. litter respiration). The turnovers of plant, litter, and soil carbon pools are 'litter production' (LP), 'litter decomposition' (LD), and 'soil respiration' (SR), respectively.

Likewise, the 'atmosphere' (A) exchanges nitrogen with the land nitrogen pools by 'nitrogen atmospheric deposition' (AD), 'biological nitrogen fixation' (BNF), 'mineral nitrogen loss that goes into atmosphere' or 'gaseous nitrogen loss' (LS2A), as well as 'land use or other anthropogenic fluxes' (LU). The turnover fluxes from plant, litter, soil, and mineral pools are 'litter production' (LP), 'litter decomposition' (LD), 'soil respiration' (SR), and 'mineral nitrogen loss' (LS), respectively. The plant takes up nitrogen from the mineral nitrogen pool ('plant uptake' - PU). The mineral nitrogen pool receives additional nitrogen from 'nitrogen fertilizer application' (FT). Considering the intended time domain of applicability, i.e., the long time step that integrates carbon cycle and nitrogen cycle dynamics over periods of one year or more, the fluxes NPP, BNF, PU, LU and the turnover fluxes lead not only to changes in the direct target pools, but also in subsequent ones. For instance, the NPP flux is simultaneously partitioned to plant, litter, and soil carbon pools by a fraction factor (f). The mass balance for the carbon pools is:

$$\frac{dC_P}{dt} = f_{NPP2P}NPP - LPR - LP_c - f_{LU2P_c}LU_c \quad (1)$$

$$\frac{dC_L}{dt} = f_{NPP2L}NPP + f_{LP2L_c}LP_c - LD_c - f_{LU2L_c}LU_c \quad (2)$$

$$\frac{dC_S}{dt} = f_{NPP2S}NPP + f_{LP2S_c}LP_c + f_{LD2S_c}LD_c - SR_c - f_{LU2S_c}LU_c \quad (3)$$

For the land carbon:

$$\frac{dC_{LAND}}{dt} = NPP - LPR - f_{LD2A}LD_c - SR_c - LU_c \quad (4)$$

The sum of $(LPR + f_{LD2A}LD_c + SR_c)$ is the heterotrophic respiration flux.

The mass balance for the four nitrogen pools is:

$$\frac{dN_P}{dt} = f_{BNF2P}BNF + f_{PU2P}PU - LP_n - f_{LU2P_n}LU_n \quad (5)$$

$$\frac{dN_L}{dt} = f_{BNF2L}BNF + f_{PU2L}PU + f_{LP2L_n}LP_n - LD_n - f_{LU2L_n}LU_n \quad (6)$$

$$\frac{dN_S}{dt} = f_{BNF2S}BNF + f_{PU2S}PU + f_{LP2S_n}LP_n + f_{LD2S_n}LD_n - SR_n - f_{LU2L_n}LU_n \quad (7)$$

$$\frac{dN_M}{dt} = AD + FT + f_{LD2M_n}LD_n + SR_n - PU - LS \quad (8)$$

For the land nitrogen:

https://doi.org/10.5194/egusphere-2024-1941
Preprint. Discussion started: 18 September 2024

$$\frac{dN_{LAND}}{dt} = BNF + AD + FT - LS - LU_n \quad (9)$$

The subscripts 'c' and 'n' for LP, LD, SR, and LU denote the carbon and nitrogen fluxes. The subscripts X2Y for the partitioning factor 'f' refer to the fraction of flux X that enters pool Y (or exits in the case of land-use). The partitioning factors, including $f_{NPP2P} + f_{NPP2L} + f_{NPP2S}$, $f_{LP2L} + f_{LP2S}$ (for both carbon and nitrogen), $f_{LU2P} + f_{LU2L} + f_{LU2S}$ (for both carbon and nitrogen), $f_{LD2S} + f_{LD2A}$ (for carbon) or $f_{LD2S} + f_{LD2M}$ (for nitrogen), $f_{BNF2P} + f_{BNF2L} + f_{BNF2S}$, and $f_{PU2P} + f_{PU2L} + f_{PU2S}$, always sum to unity.

2.3 The updated formulations for CO_2 and temperature effect on NPP

2.3.1 CO_2 fertilization

The NPP flux is modeled by scaling an initial NPP (NPP_0) with effect from CO_2 (ϵ_{CO_2}), temperature change ($\epsilon_{dT(NPP)}$), carbon-nitrogen coupling ($\epsilon_{CN(NPP)}$), and land use change (ϵ_{LU}):

$$NPP = NPP_0 \times \epsilon_{CO_2} \times \epsilon_{dT(NPP)} \times \epsilon_{CN(NPP)} \times \epsilon_{LU} \quad (10)$$

The CO_2 fertilization formulations can take multiple forms. The first, the logarithmic formulation, is adapted from (Bacastow and Keeling, 1973):

$$\epsilon_{CO_2}^{log} = 1 + s_{CO_2}^{log} \times ln\left(CO_2/CO_{2ref}\right) \quad (11)$$

where $s_{CO_2}^{log}$ represents the sensitivity of NPP to the logarithm of the ratio of current atmospheric CO_2 concentration (CO_2) to a reference CO_2 level (CO_{2ref}, e.g., the pre-industrial CO_2 concentration) (i.e., the relative change of CO_2 to CO_{2ref}).

The second, the rectangular hyperbolic formulation, is adapted from (Hunt et al., 1991; Gifford, 1993):

$$\epsilon_{CO_2}^{rect} == \frac{1/\left(CO_{2ref} - CO_{2b}\right) + s_{CO_2}^{rect}}{1/(CO_2 - CO_{2b}) + s_{CO_2}^{rect}} \quad (12)$$

where CO_{2ref} is the reference CO_2 level (e.g., the pre-industrial CO_2 concentration), the CO_{2b} is the CO_2 concentration when NPP = 0, which has a default value of 31 ppm (Gifford, 1993), and $s_{CO_2}^{rect}$ determines the CO_2 sensitivity of NPP in the rectangular hyperbolic formulation.

When the CO_2 concentration increases from 340 to 680 ppm, the ratio of the feedback factor at 680 ppm to that at 340 ppm (r) is designed to be the same for both formulations to ensure better compatibility:

$$r = \epsilon_{CO_2}^{log}(680)/\epsilon_{CO_2}^{log}(340) = \epsilon_{CO_2}^{rect}(680)/\epsilon_{CO_2}^{rect}(340) \quad (13)$$

The sensitivities of NPP in the two formulations are therefore related by:

$$r = \frac{1 + s_{CO_2}^{log} \times ln\left(680/CO_{2ref}\right)}{1 + s_{CO_2}^{log} \times ln\left(340/CO_{2ref}\right)} \quad (14)$$

$$s_{CO_2}^{rect} = \frac{(680 - CO_{2b}) - r(340 - CO_{2b})}{(r-1)(680 - CO_{2b})(340 - CO_{2b})} \quad (15)$$

https://doi.org/10.5194/egusphere-2024-1941
Preprint. Discussion started: 18 September 2024

The previous version of MAGICC uses a linear combination of the logarithmic and rectangular hyperbolic formulations to calculate the final CO_2 fertilization effect. However, because the logarithmic formulation is an unbounded function, the linear combination becomes unbounded as well unless the logarithmic formulation is removed, resulting in an overreliance on the rectangular hyperbolic formulation. The rectangular hyperbolic formulation itself can increase steeply if the CO_2 sensitivity of NPP in the rectangular formulation ($s_{CO_2}^{rect}$) is small. Considering $s_{CO_2}^{rect}$ is dependent on r (or $s_{CO_2}^{log}$, Eqs. 14 and 15), the small $s_{CO_2}^{log}$ value is easily attainable, thereby leading to a high CO_2 fertilization factor. To fix this problem, a sigmoidal CO_2 fertilization formulation is introduced and included in the updated carbon-nitrogen model presented here.

$$\epsilon_{CO_2}^{sig} = \frac{\epsilon_{CO_2max}^{sig}}{1 + \left(\epsilon_{CO_2max}^{sig} - 1\right) \times e^{-s_{CO_2}^{sig}(CO_2 - CO_{2ref})}} \tag{16}$$

where $\epsilon_{CO_2max}^{sig}$ denotes the maximum of the sigmoidal CO_2 fertilization (always >=1, which occurs when CO_2 reaches infinity) and $s_{CO_2}^{sig}$ is the CO_2 sensitivity of NPP in the sigmoidal formulation.

We allow for a linear combination of CO_2 fertilization formulations. A method factor (m_{CO_2}) ranging from 0 to 2 is used to combine the formulations and calculate the effective CO_2 feedback.

For $0 < m_{CO_2} < 1$:

$$\epsilon_{CO_2} = \left(1 - m_{CO_2}\right) \times \epsilon_{CO_2}^{log} + m_{CO_2} \times \epsilon_{CO_2}^{rect} \tag{17}$$

For $1 < m_{CO_2} < 2$:

$$\epsilon_{CO_2} = \left(2 - m_{CO_2}\right) \times \epsilon_{CO_2}^{rect} + \left(m_{CO_2} - 1\right) \times \epsilon_{CO_2}^{sig} \tag{18}$$

2.3.2 Feedback from the temperature change

Global-mean temperature change (dT) is taken as a proxy for climate-related impacts on the carbon cycle fluxes, i.e. for representing the carbon-climate feedback. The feedback of dT on NPP is assumed to be an exponential or sigmoidal scaler of NPP_0, based on a given temperature sensitivity ($s_{dT(NPP)}^{exp}$ or $s_{dT(NPP)}^{sig}$). The latter is introduced to better capture the trend of NPP in low emission scenarios. And similarly, a method factor (m_{dT}, between 0 and 1) is used to control the effective temperature change feedback on NPP.

$$\epsilon_{dT(NPP)}^{exp} = e^{s_{dT(NPP)}^{exp} \times dT} \tag{19}$$

$$\epsilon_{dT(NPP)}^{sig} = \frac{2}{1 + e^{-s_{dT(NPP)}^{sig} \times dT}} \tag{20}$$

$$\epsilon_{dT(NPP)} = (1 - m_{dT}) \times \epsilon_{dT(NPP)}^{exp} + m_{dT} \times \epsilon_{dT(NPP)}^{sig} \tag{21}$$

https://doi.org/10.5194/egusphere-2024-1941
Preprint. Discussion started: 18 September 2024

2.4 The carbon-nitrogen coupling effect on NPP

The current carbon-nitrogen coupling emphasizes the nitrogen plant uptake (PU) requirement and mineral nitrogen availability, based on which the nitrogen deficiency (or surplus) can be calculated and the subsequent influence on NPP. The direct linkage between NPP (or photosynthesis) and plant nitrogen status is a common treatment in complex carbon-nitrogen coupled models (Zaehle and Dalmonech, 2011; Zaehle et al., 2014).

The overall formulation design of the carbon-nitrogen coupling effect on NPP is as follows: First, we establish a relationship between NPP (carbon fixation) and nitrogen plant uptake (nitrogen fixation). We then calculate the potential NPP (the carbon-only NPP, NPP_C) by setting $\epsilon_{CN(NPP)} = 1$. The corresponding plant uptake requirement (PU_{req}) is determined by this NPP_C (as well as temperature effect, see details in the formulation). Nitrogen availability depends on the current mineral nitrogen pool size and fluxes (Eq. 8). The net mineralization, which is the largest source of mineral nitrogen, comes from litter and soil nitrogen turnovers. The turnovers are dependent on the pool sizes based on the first-order decay formulation. Considering that plant uptake is the predominant influx for the organic nitrogen pools (Eqs. 5-7), net mineralization is indirectly influenced by it. When approximating net mineralization as being linearly correlated with plant uptake, the unmet plant uptake requirement from net mineralization alone can be calculated as a function of the required plant uptake itself (i.e., the required plant uptake minus net mineralization = f(PU_{req})). We also include the nitrogen supply from atmospheric deposition to calculate nitrogen deficiency or surplus. This nitrogen deficiency/surplus is then converted to the nitrogen effect factor ($\epsilon_{CN(NPP)}$) and used to update the carbon-nitrogen coupled NPP (NPP_{CN}, Eq. 10). The actual plant uptake (PU_{act}) is correspondingly updated based on the NPP_{CN}. The following describes the detailed formulations.

First, we assume that the nitrogen plant uptake is a function of the NPP (whether potential or actual) and scaled by the temperature feedback on plant uptake ($\epsilon_{dT(PU)}$):

$$PU = PU_{max} \times e^{-\frac{NPP_{ref}}{NPP}} \times \epsilon_{dT(PU)} \quad (22)$$

$$\epsilon_{dT(PU)} = e^{s_{dT(PU)} \times dT} \quad (23)$$

where NPP_{ref} is a reference NPP used to normalize the real time NPP (further explanation in the next paragraph), PU_{max} sets the upper bound of the plant uptake without the temperature feedback, and $s_{dT(PU)}$ is the temperature sensitivity of plant uptake.

When NPP = NPP_{ref}, with $dT = 0$, the plant uptake is fixed to PU_{max}/e. The PU_{max} and NPP_{ref} parameter pair defines a unique plant carbon-nitrogen assimilation system. Specifically, $PU_{max}/(e \times NPP_{ref})$ reflects a default setting of the plant nitrogen:carbon ratio. It is also worth reiterating that NPP_{ref} is not necessarily the same as the initial NPP (NPP_0 in Eq. 10).

The formulation presented in Eq. 22 suggests an increasing plant uptake with increasing NPP. However, as NPP increases, the plant uptake needed per additional unit NPP gradually decreases. This provides a way for the model to represent a declining carbon:nitrogen ratio in plant biomass with increasing NPP due to, for example, CO_2 fertilization.

https://doi.org/10.5194/egusphere-2024-1941
Preprint. Discussion started: 18 September 2024

When nitrogen effect is not considered, NPP can reach its potential value, the carbon-only NPP (NPP_C), which can be calculated using Eq. 10 (fixing $\epsilon_{CN(NPP)} = 1$). The corresponding nitrogen plant uptake requirement (PU_{req}) can be calculated based on Eq. 22:

$$PU_{req} = PU_{max} \times e^{-\frac{NPP_{ref}}{NPP_C}} \times \epsilon_{dT(PU)} \quad (24)$$

The integration of the required plant uptake over a certain time period (e.g., the model time step) indicates the mineral nitrogen needed for the potential NPP. On the other hand, the available mineral nitrogen for plant uptake is determined by the current nitrogen pool size, which is dependent on several nitrogen influxes, including atmospheric deposition (AD), nitrogen fertilizer use (FT), and net mineralization (mineralization minus immobilization), and outfluxes like nitrogen losses (LS) and plant uptake (PU) (Eq. 8).

The nitrogen mineralization or net mineralization (mineralization minus immobilization) and atmospheric deposition are the natural sources enriching the mineral nitrogen pool. The net mineralization is the largest mineral nitrogen supply, which is a key flux for determining the nitrogen limitation of NPP. The net mineralization comes from the litter and soil nitrogen turnovers. As all the turnovers in MAGICC's carbon and nitrogen pools are assumed to follow first-order decay, the net mineralization is dependent on the litter and soil nitrogen pool sizes - or more generally - the land organic nitrogen pool size.

Biological nitrogen fixation and plant uptake are the two influxes that lead to accumulation of land organic nitrogen. On a yearly scale, plant uptake is the predominant source for the organic nitrogen pools (5 to >10 times greater than biological nitrogen fixation in the complex models we have examined). Effectively, plant uptake controls the accumulation of nitrogen in plant, litter, and soil pools. As we assume a first order decay of the organic nitrogen pools, it also means that the net mineralization is indirectly affected by plant uptake. In other words, plant uptake and net mineralization, the two major fluxes channeling through the organic and inorganic nitrogen pools by either consuming mineral nitrogen to enrich organic nitrogen or vice versa, are closely intertwined and mutually influence each other. This is supported by the results from complex models (CABLE, OCN, and multiple CMIP6 models) that show similar value and trend for net mineralization and plant uptake at the global-mean, annual-mean level.

When approximating the net mineralization as being linearly correlated with plant uptake, the unmet plant uptake requirement from net mineralization alone can then be a linear function of the required plant uptake itself (i.e., the required plant uptake minus net mineralization = $f_2 \times PU_{req}$ where f_2 is a constant). Considering that atmospheric deposition also supports the plant uptake requirement, its effect of alleviating the nitrogen deficiency is added by another linear function ($f_1 \times AD$). The carbon-nitrogen coupling effect on NPP ($\epsilon_{CN(NPP)}$) is then determined by:

$$\epsilon_{CN(NPP)} = \epsilon_{CN(NPP)0} \times e^{f_1 \times AD - f_2 \times PU_{req}} \quad (25)$$

Where $\epsilon_{CN(NPP)0}$ is a base nitrogen effect on NPP when there is neither deficiency nor surplus. f_1 and f_2 are fitted parameters whose values are always positive. The $(f_1 \times AD - f_2 \times PU_{req})$ term determines the relative strength of the current nitrogen deposition and unmet nitrogen plant uptake requirement (nitrogen deficiency/surplus).

https://doi.org/10.5194/egusphere-2024-1941
Preprint. Discussion started: 18 September 2024

This formulation is transformed from complex models with the key idea of comparing mineral nitrogen availability and plant nitrogen requirement. In complex carbon-nitrogen models, the nitrogen availability is typically based on the current mineral nitrogen pool size (with mass unit) and the nitrogen requirement is computed from the integrated fluxes in a given time step (with mass unit) (Thornton et al., 2007; Wiltshire et al., 2021; Zaehle et al., 2014). The competition from microbial immobilization is also considered in some complex models. However, in a model with a much longer time step (e.g., annually) like ours, such a system would be inherently unstable since the mineral nitrogen pool size would be orders of magnitude smaller than the annual nitrogen demand (i.e., the system would be unstable because the turnover of the mineral nitrogen pool would be substantially smaller than the time-step).

Fixing f_1 = 1 indicates that on the timescale of interest (e.g., yearly), all mineral nitrogen from AD is 100% available for the plant. However, this is not necessarily correct considering that 1) the process-level nitrogen limitation/fertilization does not remain constant over the timescale of interest (e.g., yearly); 2) the mineral nitrogen accumulation from previous time steps can be used for the current plant uptake; and 3) the direct mineral nitrogen loss, whose magnitude is determined by the mineral pool turnover time, may counterbalance the effect of nitrogen deposition on the fertilization. Therefore, giving freedom to both the f_1 and f_2 parameters implicitly allows our formulation to consider the above effects.

Note that both f_1 and f_2 parameters are calibrated, the $\epsilon_{CN(NPP)}$ does not necessarily have to be $\epsilon_{CN(NPP)0}$ at the start of the experiments, which gives flexibility to the model to determine the carbon-nitrogen coupling effect in the pre-industrial condition.

After the nitrogen effect is calculated, the NPP with the carbon-nitrogen coupling effect (NPP_{CN}) is determined by:

$$NPP_{CN} = NPP_C \times \epsilon_{CN(NPP)} \tag{26}$$

And the corresponding actual plant uptake (PU_{act}) becomes:

$$PU_{act} = PU_{max} \times e^{-\frac{NPP_{ref}}{NPP_{CN}}} \times \epsilon_{dT(PU)} \tag{27}$$

2.5 The plant litter production respiration flux

MAGICC separately simulates a 'plant litter production respiration' flux (LPR, the fast litter respiration produced from the plant litter production that does not carry over into the subsequent year i.e. that returns to the atmosphere on sub-annual timescales) by scaling an initial plant litter production respiration flux (LPR_0) with the CO_2 fertilization effect (ϵ_{CO_2}), the carbon-nitrogen coupling effect on NPP ($\epsilon_{CN(NPP)}$), the climate effect ($\epsilon_{dT(LPR)}$), and the land use change effect (ϵ_{LU}).

$$LPR = LPR_0 \times \epsilon_{CO_2} \times \epsilon_{dT(PR)} \times \epsilon_{CN(NPP)} \times \epsilon_{LU} \tag{28}$$

$$\epsilon_{dT(LPR)} = e^{s_{dT(LPR)} \times dT} \tag{29}$$

The plant litter production respiration flux is assumed to be a fast over-turning (e.g., within one-year) outflux from the plant carbon pool that is circulating through the NPP to plant to litter to atmosphere. Considering the close relationship between plant litter production respiration flux and NPP, it is scaled by the same CO_2 and carbon-nitrogen coupling feedback as NPP,

https://doi.org/10.5194/egusphere-2024-1941
Preprint. Discussion started: 18 September 2024

as well as the same land use effect. The plant litter production respiration flux has its own exponential temperature response based on its own temperature sensitivity ($s_{dT(LPR)}$).

2.6 The turnover of carbon and nitrogen pools

The litter production (LP), litter decomposition (LD), and soil respiration (SR) for plant, litter, and soil carbon/nitrogen pools are assumed to be proportional to the corresponding pool sizes, linked by the turnover time and scaled by the effect from temperature change and carbon-nitrogen coupling. The nitrogen loss (LS) is the turnover flux for the mineral nitrogen pool. However, only temperature effect is applied to nitrogen loss since the current atmospheric decomposition and plant uptake, two proxies for the carbon-nitrogen feedback, are already directly the influx and outflux for the mineral pool.

$$LP_c = \frac{C_P}{\tau_{C_P}} \times \epsilon_{dT(LP_c)} \times \epsilon_{CN(LP_c)} \quad (30)$$

$$LD_c = \frac{C_L}{\tau_{C_L}} \times \epsilon_{dT(LD_c)} \times \epsilon_{CN(LD_c)} \quad (31)$$

$$SR_c = \frac{C_S}{\tau_{C_S}} \times \epsilon_{dT(SR_c)} \times \epsilon_{CN(SR_c)} \quad (32)$$

$$LP_n = \frac{N_P}{\tau_{N_P}} \times \epsilon_{dT(LP_n)} \times \epsilon_{CN(LP_n)} \quad (33)$$

$$LD_n = \frac{N_L}{\tau_{N_L}} \times \epsilon_{dT(LD_n)} \times \epsilon_{CN(LD_n)} \quad (34)$$

$$SR_n = \frac{N_S}{\tau_{N_S}} \times \epsilon_{dT(SR_n)} \times \epsilon_{CN(SR_n)} \quad (35)$$

$$LS = \frac{N_M}{\tau_{N_M}} \times \epsilon_{dT(LS)} \quad (36)$$

For the temperature feedback, it is assumed that each process has its own temperature sensitivity. The feedback is then an exponential relationship with them.

$$\epsilon_{dT(i)} = e^{s_{dT(i)} \times dT} \quad (37)$$

where *i* is the turnover processes litter production (LP), litter decomposition (LD) and soil respiration (SR) for both carbon and nitrogen pools and also nitrogen loss (LS) for the mineral nitrogen pool.

The carbon-nitrogen coupling feedback takes current PU and atmospheric deposition as proxies to represent the plant nitrogen status and the nitrogen forcing, respectively. And similarly, each turnover process has its own response to the current plant uptake ($s_{PU(i)}$) and atmospheric deposition ($s_{AD(i)}$). An exponential relationship is used to simulate their effects on the processes.

$$\epsilon_{CN(i)} = e^{s_{PU(i)} \times PU} \times e^{s_{AD(i)} \times AD} \quad (38)$$

https://doi.org/10.5194/egusphere-2024-1941
Preprint. Discussion started: 18 September 2024

where *i* is the turnover processes litter production (LP), litter decomposition (LD), and soil respiration (SR) for both carbon and nitrogen pools.

2.7 The updated implementation of land use emissions and their impact on NPP

Most scenarios run in MAGICC, for example those in AR6 (see Mitigation pathways compatible with long-term goals. In IPCC, 2022: Climate Change 2022: Mitigation of Climate Change), directly report the net land use emissions (gross deforestation - regrowth) instead of the separation of those two parts. Considering a box model with fixed turnover times, when the input is constant (e.g., constant NPP), a one-off subtraction of carbon out of one of the pools (e.g., a one-off gross deforestation) would not lead to a permanent reduction in the amount of carbon in this pool. Instead, it would yield an asymptotic approach to the pre-intervention carbon pool size over time (as the carbon that was moved out of the pool is taken up by the land again), which implies full regrowth in the long term. In MAGICC's previous carbon cycle, the partial regrowth was accounted for using a factor that determines the fraction of expected regrowth and adjustments to the turnover times (Meinshausen et al., 2011a). This implementation blends the regrowth with changes in the pool's turnover fluxes. As the turnovers are also impacted by feedbacks (Eqs. 30-36), the previous MAGICC setup required a parallel calculation of the non-feedback case to retrieve the regrowth flux and correctly handle the land-use input.

The updated land use emission implementation described here makes the regrowth and gross deforestation more straightforward. The LU input in Eqs. 1-4 refers to the net land use emissions, which can be written as:

$$LU_c = LU_{grsd} - LU_{rgr} \tag{39}$$

where LU_{grsd} and LU_{rgr} refer to the gross deforestation (instantaneous biomass extraction from land organic carbon pool) and regrowth (legacy biomass addition to land organic carbon pool), respectively.

The regrowth formulation assumes a constant regrowth flux during the growing years following each instance of gross deforestation. Therefore, the regrowth flux is calculated as the total regrowth (part of the gross deforestation) divided by the regrowth time, formulated as follows:

$$LU_{rgr} = \frac{\varphi \int_{max(0,t-\tau_{rgr})}^{t} LU_{grsd}}{\tau_{rgr}} \tag{40}$$

where φ refers to the fraction of gross deforestation that can regrow; τ_{rgr} denotes the regrowth time required to reach the partial regrowth.

The formulation assumes a constant regrowth flux (LU_{rgr}) for τ_{rgr} years after every single gross deforestation - the regrowth flux at time t is thus the potential total regrowth (φ times the integration of LU_{grsd}) divided by the required regrowth time (τ_{rgr}).

Note that, in this formulation for regrowth and gross deforestation, both fluxes exist only within a certain time period (τ_{rgr}), hence they cannot change the long-term equilibrium of the system because the fixed turnover times always return the system to its pre-deforestation state (Eqs. 1-4). Instead of adjusting the turnover times (as in previous versions of MAGICC), the

https://doi.org/10.5194/egusphere-2024-1941
Preprint. Discussion started: 18 September 2024

updated MAGICC applies the effect of land use change to NPP to change the long-term equilibrium after the gross deforestation (ϵ_{LU} in Eq. 10), which is formulated as:

$$\epsilon_{LU} = \frac{C_{LAND_0} - (1-\varphi)\int_0^t LU_{grsd}}{C_{LAND_0}} \tag{41}$$

where C_{LAND_0} is the initial land carbon pool size.

The land use effect on NPP assumes that the NPP is reduced immediately after gross deforestation activities. Considering the simultaneous regrowth, the NPP reduction is proportional to the accumulated permanent gross deforestation $[(1-\varphi)\int_0^t LU_{grsd}]$. With the land use effect on NPP, when there is a one-off gross deforestation, the NPP gradually decreases to reach a value depending on the regrowth fraction φ (e.g., $\varphi = 0$ refers to zero-regrowth and the gross deforestation causes permanent carbon loss from the land carbon pools). Because of such NPP change, the long-term equilibrium of the system changes accordingly to account for the effect of partial regrowth after deforestation without altering the turnover times of carbon pools.

The new formulation enables the separate calculation of regrowth and gross deforestation without the non-feedback run. Arguably, it also makes more physical sense, because deforestation reduces the amount of forest (area) available to grow and hence the amount of NPP. The applied effect on NPP also means an additional constraint on MAGICC's simulation of regrowth and gross deforestation. The LU input must be consistent with the complex model outputs, the scenarios, and some definitions of land use change emissions (e.g., ELUC in the Global Carbon Budget project). However, it should be noted that the definition discrepancy of land use change emissions itself still exists among different models/approaches and is leading to substantial differences in land-use emission estimates (Gasser and Ciais, 2013; Stocker and Joos, 2015). It should also be noted that MAGICC does not simulate the carbon or nitrogen storage in the product pool due to its relatively small size (Eqs. 1-9 and Fig. 1). Thus, the deforestation and harvest fluxes going into the product pool, expected to be small, are accounted for in the land use emission input (LU_c or LU_n), while the land carbon (or nitrogen) pool does not include the correspondingly stored carbon (or nitrogen) within the product.

https://doi.org/10.5194/egusphere-2024-1941
Preprint. Discussion started: 18 September 2024

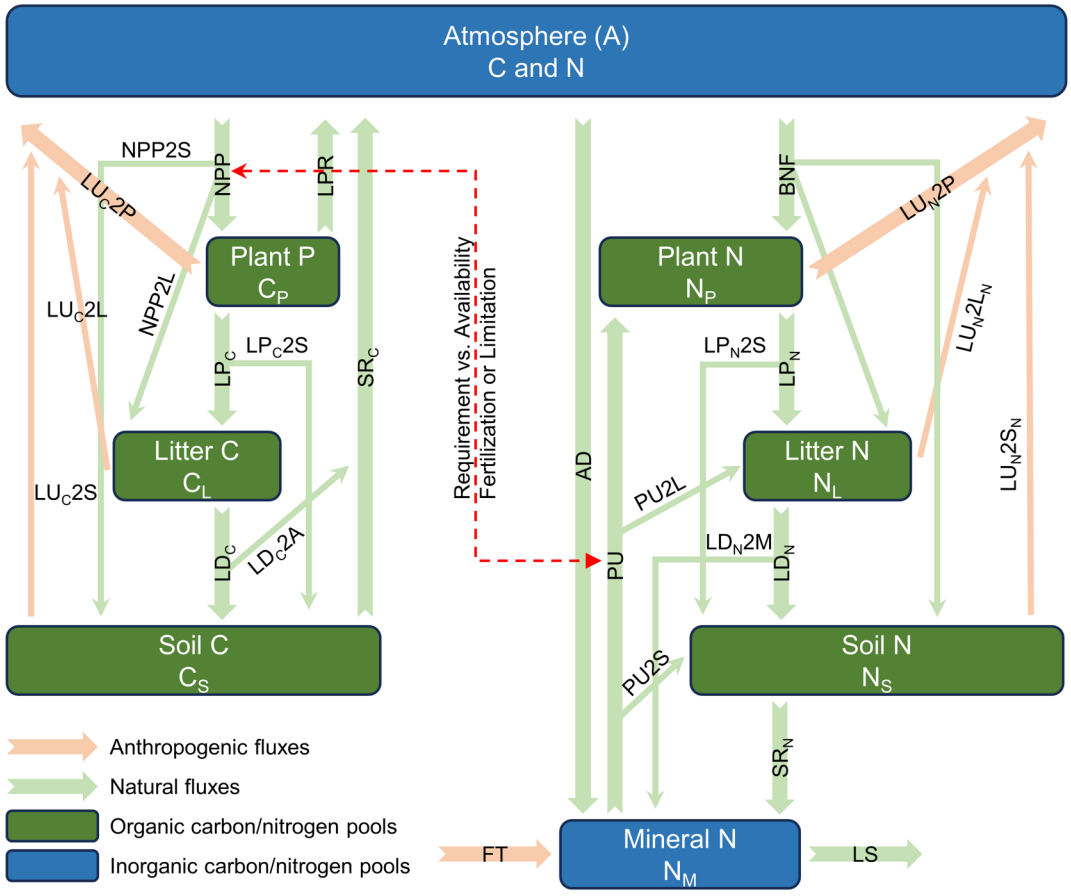

Figure 1. The coupled carbon-nitrogen cycle in MAGICC (NPP: net primary production, LPR: plant litter production respiration, PU: nitrogen plant uptake, BNF: biological nitrogen fixation, LP: litter production, LD: litter decomposition, SR: soil respiration, LS: mineral nitrogen loss, LU: land use emission, AD: atmosphere nitrogen deposition, FT: nitrogen fertilizer application, 2P, 2L, 2S, and 2M: the partition of fluxes into plant, litter, soil, and mineral pools).

3 Model calibration

3.1 Data acquisition and processing

The CABLE and OCN land surface model output datasets (global-, annual-mean values) were obtained directly from the modeling groups. CABLE is the land surface component for the Australian Community Climate and Earth System Simulator (ACCESS-ESM1) (Law et al., 2017) and ACCESS-CM2 (Bi et al., 2020). OCN is the updated land surface model built on ORCHIDEE (Zaehle and Friend, 2010), the land surface component of the IPSL-CM climate model (Boucher et al., 2020). Both CABLE and OCN provided the results from the carbon-only and carbon-nitrogen coupled setups for the representative concentration pathway 8.5 (RCP85) scenario (Fleischer et al., 2019), with OCN also providing the results for the RCP26 scenario (Meyerholt et al., 2020). The data from both the carbon-only and carbon-nitrogen coupled setups of the land surface

https://doi.org/10.5194/egusphere-2024-1941
Preprint. Discussion started: 18 September 2024

models offers valuable information to constrain nitrogen interactions separately from the climate and CO_2 effects. Unfortunately, a robust and feedback-specific emulation is not feasible for CMIP6 ESMs, as the results from experiments without the nitrogen effect are unavailable. The carbon-nitrogen coupled runs in CABLE consisted of two experiments with constant and dynamic atmospheric deposition inputs, respectively (Fleischer et al., 2019). These experiments are useful for diagnosing the standalone effect of atmospheric deposition. The climate data and atmosphere CO_2 concentration for the land surface model experiments were derived either from their corresponding ESM outputs (Meyerholt et al., 2020) or the RCP greenhouse gas concentrations (Meinshausen et al., 2011b). One OCN model structure with flexible carbon:nitrogen ratio, linear biological nitrogen fixation and actual evaporation relationship, and explicit mineral nitrogen loss representation - namely the FLX/FOR/NL1 structure - from the 30 ensemble model structures in the original paper was selected for the MAGICC calibration in this paper (Meyerholt et al., 2020). The selected OCN model structure serves as a proof-of-concept for the proposed MAGICC carbon-nitrogen cycle. Future work will explore alternative structures and address structural uncertainties.

The CMIP6 model outputs were downloaded from Earth System Grid Federation (ESGF, https://esgf-node.llnl.gov/projects/cmip6/, last access, January 18, 2024) and processed/aggregated into global-mean, annual-mean values. Briefly, we first collected all the monthly gridded data for the C4MIP required carbon-nitrogen pool and flux variables from different ESMs and different experiments. The selection of ESMs and experiments is based on the following criteria: 1) The model includes a terrestrial nitrogen cycle; 2) The outputs encompass the majority of carbon-nitrogen cycle variables needed for C4MIP; and 3) The model has completed all selected experiments, including one idealized experiment (1pctCO2), historical simulations (historical), and four Shared Socioeconomic Pathways (SSPs) scenarios (SSP126, SSP245, SSP370, and SSP585), all of which are CMIP6 tier 1 concentration-driven experiments. Based on the data availability and completeness, the ESMs chosen for the calibration included: CMCC-CM2-SR5 (land: CLM4.5) (Cherchi et al., 2019), CMCC-ESM2 (land: CLM4.5, BGC configuration) (Lovato et al., 2022), MPI-ESM1-2-LR (land: JSBACH3.2) (Mauritsen et al., 2019), NorESM2-LM (land: CLM5) (Seland et al., 2020), UKESM1-0-LL (land: JULES-ES-1.0) (Sellar et al., 2019), MIROC-ES2L (land: VISIT-e) (Hajima et al., 2020). Our grid-to-global aggregation used the model-specific grid area (areacella) and land fraction (sftlf) to avoid issues with the resolution variation across different model outputs. Our monthly-to-annual aggregation first concatenated the original monthly outputs along the time dimension and then calculated the annual values, weighted by the number of days in each month as defined by each ESM's output calendar. It should be noted that, even though the selected ESMs and experiments provided relatively complete outputs for the pools and fluxes, none of them reported all the required fluxes by C4MIP, especially those related to the land use and anthropogenic perturbations. As part of the processing, it was not trivial to reproduce the models' mass balance based on the reported outputs. Investigation into this issue is ongoing. For this paper, we have applied a workaround, which we describe in the next section.

https://doi.org/10.5194/egusphere-2024-1941
Preprint. Discussion started: 18 September 2024

3.2 Calibration setup

The targets set for both the land surface models and CMIP6 ESMs calibration included all the carbon/nitrogen pool sizes, NPP, heterotrophic respiration, and plant uptake fluxes. For CABLE and OCN, the forcing data was provided by the original
395 providers. For the CMIP6 ESMs calibration, the temperature data was taken from ESM outputs (tas in C4MIP and CMIP6) and the CO_2 concentrations were taken from the CMIP6 forcing datasets (Meinshausen et al., 2017; Meinshausen et al., 2020). The carbon-nitrogen cycle uses temperature change (dT) as a proxy for climate-related impact, calculated as the difference between the current temperature and the initial year temperature.

We used the global-mean temperature change provided by the respective models as an input to the offline calibration - using
400 the first year as the base period. For the CMIP6 ESMs, the results from the historical period and SSP scenarios were combined (referred to as hist_SSP for simplicity), resulting in a unified time axis of 1850-2100 or 1850-2300 (based on data availability). The biological nitrogen fixation, atmospheric decomposition, and fertilizer application fluxes were taken from the CMIP6 ESM outputs and utilized as inputs for MAGICC's carbon-nitrogen cycle. The land-use flux was also imputed from the CMIP6 ESM output and supplied directly into the carbon-nitrogen cycle. To input the land-use flux, we calculated
405 the imbalance between carbon pool size change and the accumulated "NPP minus heterotrophic respiration". This imbalance was used as the LU_c input in the carbon-nitrogen cycle model (Fig. 1 and Eqs. 1-4) to ensure that mass was conserved (which is not trivial from the reported outputs alone, see Investigating the Mass Imbalance in CMIP6 Carbon-Nitrogen Cycle Data, in preparation). Where available, land use and anthropogenic disturbance-related nitrogen fluxes (fNAnthDisturb and fNProduct in CMIP6 Data Request) are summed together to form the LU_n input in the carbon-nitrogen cycle model (Fig. 1
410 and Eqs. 5-9).

The parameter calibration applied the differential evolution algorithm (Storn and Price, 1997) for global optimization and the Nelder-Mead algorithm (Gao and Han, 2012) for local minimization. The calibration process comprised 30,000 iterations of the differential evolution algorithm under ten different random initializations. The resulting ten sets of global-minimum parameters were then employed as initial guesses for the Nelder-Mead algorithm to get their respective local minimums.
415 Finally, the parameter set resulting in the lowest 'root mean squared error' (RMSE) across all normalized time series differences was selected as the best-estimate parameter set. The full parameter list and the best-estimate values were provided in Table A1 in the Appendix.

3.3 Calibrating MAGICC to CABLE and OCN

The carbon-nitrogen coupled MAGICC has successfully emulated the fluxes and pool sizes from the CABLE and OCN
420 experiments (Fig. 2 and Fig. A1), with the RMSE (or normalized RMSE) ranging from 0.9-2.6 GtC/yr (1.3-2.2%) for NPP, 4.0-32.9 GtC (0.2-1.0%) for land carbon pool size, 0.016-0.020 GtN/yr (1.1-1.9%) for plant nitrogen uptake, 0.05-0.11 GtN (<0.1%) for land organic nitrogen pool size, and 0.0022-0.026 GtN (2.3-6.2%) for the mineral nitrogen pool size, respectively. There is a strong and increasing nitrogen limitation on NPP in CABLE, inhibiting NPP by 9.4% to 48.2%

https://doi.org/10.5194/egusphere-2024-1941
Preprint. Discussion started: 18 September 2024

(constant atmospheric deposition) or 46.2% (dynamic atmospheric deposition) from 1901 to 2100. The total land carbon storage, i.e. the total amount of carbon taken up by the land carbon cycle, by 2100 under the RCP85 scenario in the constant and dynamic atmospheric deposition experiments is 353 GtC and 398 GtC, respectively, which is significantly lower than the 1634 GtC land carbon storage in the carbon-only experiment. The large reduction in NPP (influx of the system, Fig. 2) by the carbon-nitrogen coupling, along with the relatively smaller reduction in heterotrophic respiration (major outflux of the system, Fig. A1), result in the decrease of net land carbon flux (Fig. 2) and thus, the decreased land carbon storage (Fig. 2).

The OCN model exhibits significantly lower nitrogen limitation on NPP (< 5.0% inhibition) for both the RCP85 and RCP26 scenarios. This disparity may be attributed to the fact that the NPP in OCN in the carbon-only simulations (~85 GtC/yr in 2100 in RCP85) is notably lower than that in CABLE (~140 GtC/yr in 2100 in RCP85). The carbon cycle in OCN has also experienced a higher temperature change (~8°C from 1850 to 2100 in RCP85, Fig. A2) compared to CABLE (~5.5°C from 1900 to 2100 in RCP85, Fig. A2). The emulation captures the varied NPP increases by applying a stronger CO_2 fertilization effect and a more negative climate feedback in CABLE than in OCN. These respective changes are captured in MAGICC by the logarithmic carbon-concentration feedback formulation with a high sensitivity ($s_{CO_2}^{log}$ = 2.582) and negative $s_{dT(NPP)}^{exp}$ and $s_{dT(NPP)}^{sig}$ parameters (Table A1). Nevertheless, the relatively minor NPP limitation in OCN, along with the resulting decrease in net land carbon flux (Fig. 2), lead to a reduction of 45 GtC (or 10%, RCP85) and 26 GtC (or 8%, RCP26) in land carbon storage by the end of 2100 compared to their respective carbon-only simulations.

In the RCP85 experiment, CABLE and OCN show similar relative changes in plant uptake over time; however, their starting plant uptake fluxes differ (~0.6-1.0 GtN/yr in CABLE vs ~1.0-1.4 GtN/yr in OCN). The emulation is able to capture both dynamics by adjusting the maximum plant uptake (PU_{max}) and temperature sensitivity of plant uptake ($s_{dT(PU)}$) parameters. Specifically, the different starting plant uptake values stem from the higher maximum plant uptake in OCN (2.4 GtN/yr) than in CABLE (1.9 GtN/yr). The similar trends occur because of the higher temperature sensitivity of plant uptake in CABLE compared to OCN (0.014 K^{-1} vs 0.008 K^{-1}, Table A1), which compensates for the effect of its lower maximum plant uptake (Eqs. 22-23). In the dynamic atmospheric deposition experiment, the plant uptake in CABLE is slightly higher than in the constant atmospheric deposition experiment, primarily accumulating in the soil organic nitrogen pool (+3 GtN in 2100 compared to the constant atmospheric deposition scenario, Fig. A1). The higher plant uptake also enriches the mineral nitrogen pool instead of stimulating the nitrogen loss, as the system remains nitrogen limited. In contrast, in the RCP85 experiment from OCN, the new organic nitrogen is mainly stored in the plant pool (Fig. A1). The trend and magnitude of the mineral nitrogen pool size in OCN are also largely different from those in CABLE. The emulation captures the diverse mineral nitrogen trends by adapting the temperature response of mineral nitrogen loss for the two models (weak and negative -0.007 K^{-1} in CABLE vs strong and positive 0.088 K^{-1} for OCN, Table A1). The order-of-magnitude difference in mineral nitrogen pool sizes demonstrates the huge uncertainty in estimated mineral nitrogen quantities.

Comparing the behavior of the nitrogen cycle in OCN's RCP85 and RCP26 experiments, it is found that plant uptake follows the trend of NPP, supporting our assumption that plant uptake can be modeled based on NPP (Eq. 22). However, unlike in

https://doi.org/10.5194/egusphere-2024-1941
Preprint. Discussion started: 18 September 2024

the RCP85 scenario, the new nitrogen introduced by plant uptake is mainly accumulated in the soil nitrogen pool in the RCP26 scenario (Fig. A1). Based on the formulation, the larger soil nitrogen pool size implies more nitrogen mineralization (the first-order turnover, Eq. 35), enabling the emulation to capture the increasing trend of mineral nitrogen pool size from 2050 to 2100 (Fig. A1). The organic nitrogen accumulation in the RCP85 and RCP26 experiments does not precisely follow their corresponding carbon storage trends, where the new carbon introduced by NPP is predominantly stored in the plant carbon pool in both scenarios. This difference indicates that the carbon cycle and nitrogen cycle, even though closely intertwined, may react in a divergent manner to climate change.

https://doi.org/10.5194/egusphere-2024-1941
Preprint. Discussion started: 18 September 2024

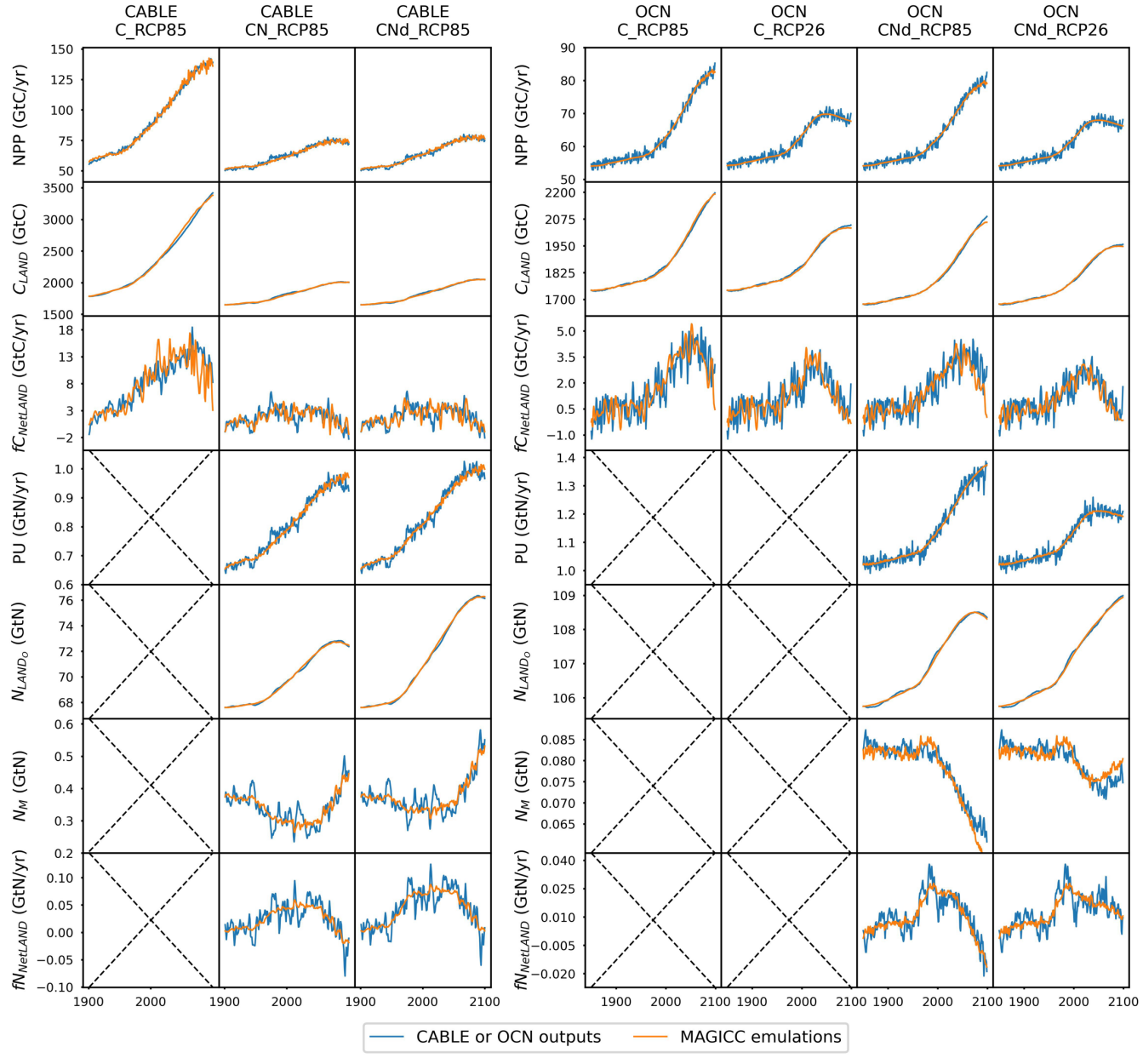

Figure 2. Comparison of net primary production (NPP), land carbon pool size (C_{LAND}), net land carbon flux ($fC_{NetLAND}$), nitrogen plant uptake (PU), land organic nitrogen pool size (N_{LANDo}, sum of nitrogen in plant, litter, and soil pools), mineral nitrogen pool size (N_M), and net land nitrogen flux ($fN_{NetLAND}$) between CABLE or OCN outputs (blue lines) and MAGICC emulations (orange lines). The experiments labeled as C, CN, and CNd denote the carbon-only, carbon-nitrogen coupled with constant nitrogen atmospheric deposition, and carbon-nitrogen coupled with dynamic nitrogen atmospheric deposition configurations in the land surface models, respectively.

https://doi.org/10.5194/egusphere-2024-1941
Preprint. Discussion started: 18 September 2024

3.4 Calibrating MAGICC to CMIP6 ESMs

MAGICC emulation captures the dynamics of major fluxes and pool sizes for all the CMIP6 ESMs and experiments (Fig. 3), despite the diverse climate and CO_2 forcings (Fig. A3). More detailed comparisons of ESM outputs and MAGICC emulations are provided in Fig. A4. In the 1pctCO2 experiment, the emulated NPP is lower than that from the UKESM1-0-LL and MIROC-ES2L outputs. The underestimation is mainly from the inconsistent behavior of these two ESMs in the idealized 1pctCO2 experiment and hist_SSP experiments. Both ESMs have simulated higher NPP at the end of their 1pctCO2 runs (~100 GtC/yr in 1999 for both ESMs) than that at the end of their SSP runs (e.g., SSP126, <80 GtC/yr in 2100 for both ESMs), which is contradictory to their plant uptake results (lower in 1pctCO2 and higher in SSPs, Fig. A4). Such behavior is in direct contradiction with our assumption that higher NPP requires a higher PU (section 2.4, Eq. 26). Since NPP and PU are both set as calibration targets, MAGICC has tried to minimize the gap between the emulated fluxes and targets, resulting in the simultaneous underestimation of NPP and overestimation of nitrogen plant uptake for UKESM1-0-LL and MIROC-ES2L (Fig. 3 and Fig. A4). However, such different behavior is only observed in the 1pctCO2 experiments for these two ESMs, indicating there could be either some model response nonlinearities between their 1pctCO2 and SSP runs that our model is not capturing or some regional distinct effects that we are not seeing in the global, annual averages.

The underestimated NPP in the 1pctCO2 experiment has led to an underestimation of ~190 GtC of the land carbon pool size for MIROC-ES2L (Fig. A4). But the underestimation of emulated land carbon in UKESM1-0-LL is much narrower (~78 GtC, Fig. A4). This is because the MAGICC emulation has overestimated the soil carbon storage at the later phase of the 1pctCO2 experiment, which compensates for some carbon loss by the underestimated NPP. The emulated land carbon pool sizes (specifically the plant carbon pool sizes) are slightly but systematically smaller than the outputs from CMCC-CM2-SR5 and CMCC-ESM2 in their 1pctCO2 runs (Fig. A4). Such results primarily stem from MAGICC's underestimation of NPP during the middle of the 1pctCO2 experiment (Fig. A4). MAGICC's emulation of pool turnovers also contributes to the inconsistency between the emulation results and ESM outputs. The first-order decay of carbon pool turnover (Eqs. 30-32) is not particularly effective in modeling the minor changes in pool sizes relative to the substantial initial pool size. For example, both CMCC models exhibit a soil carbon loss of approximately 45 GtC in their 1pctCO2 runs, with an initial soil pool size of around 2870 GtC. Consequently, the calibration has prioritized achieving better fit for soil pool sizes at the expense of accurately representing plant and litter pool sizes. The different starting soil pool sizes for ESMs' 1pctCO2 and historical simulations further complicate the soil carbon turnover emulation (Fig. A4). These different initial pool sizes in CMIP6 data do not make much sense. However, without explicit reasons to discredit the data, we have not adjusted our model to accommodate such oddities; rather, they compromise the model's fit.

The net land carbon flux is a highly variable flux (<10 GtC/yr for all the ESMs, Fig. A4). MAGICC's emulation of the ESMs has both positive and negative errors (Fig. 3). The MAGICC emulation has captured both their trends and magnitudes (Fig. A4).

https://doi.org/10.5194/egusphere-2024-1941
Preprint. Discussion started: 18 September 2024

The new nitrogen cycle in MAGICC has demonstrated the ability to capture the dynamics of nitrogen fluxes and pools, especially the nitrogen plant uptake flux and land organic nitrogen pool, in the ESM's SSP scenario runs (Fig. 3). In the 1pctCO2 experiment, however, the emulated plant uptake is overestimated for UKESM1-0-LL and MIROC-ES2L, which is accompanied by the underestimation of their NPP, in an attempt to compensate for the conflicting high NPP and low plant uptake in the ESMs' outputs (Fig. A4). The emulated organic nitrogen pool size is overestimated for NorESM2-LM (Fig. A4), which is primarily attributed to the overestimated plant uptake and soil nitrogen pool sizes (Fig. A4).

The mineral nitrogen pool sizes exhibit the most diverse results between the MAGICC emulation and the ESM outputs (Fig. 3, details in Fig. A4). Firstly, the mineral nitrogen pool sizes in UKESM1-0-LL are relatively well-emulated. Secondly, the emulated mineral nitrogen pool sizes show significant differences compared to NorESM2-LM outputs, both in magnitudes and trends. Considering that both the plant uptake flux and the organic nitrogen pool size in NorESM2-LM are relatively well-emulated (Fig. A4), such differences in mineral nitrogen pool size could be attributed to either the input nitrogen fertilizer use flux (FT) or the turnover flux (LS) of the mineral pool. MAGICC's emulation of mineral nitrogen turnover is a first order decay with an exponential temperature effect scaling (Eq. 36). Thus, the initial pool size and turnover time determine the magnitude of the nitrogen loss flux. Among all the studied CMIP6 ESMs, NorESM2-LM has the largest initial mineral nitrogen pool (5.64 GtN vs <1.50 GtN for all the other ESMs), which can lead to a large turnover flux. Conversely, the pool size change of mineral nitrogen is not significant in NorESM2-LM (0.78 GtN for 1pctCO2 and <0.35 GtN for all the hist_SSPs throughout the entire duration of the simulation). The large flux and small pool size change are naturally incompatible with each other in a first-order decay assumption, indicating uncaptured nonlinearities of the mineral pool simulation in NorESM2-LM. And lastly, the MAGICC emulation has effectively captured the trends in mineral nitrogen pool sizes simulated in CMCC-CM2-SR5, CMCC-ESM2, MPI-ESM1-2-LR, and MIROC-ES2L across all experiments (Fig. A4). Overall, the mineral pool is only a small part of the land nitrogen pool (the mineral to organic nitrogen ratio across the time series was 0.23-0.31%, 0.24-0.31%, 1.36-2.80%, 2.05-2.53%, 0.06-0.19%, and 0.14-0.43% for CMCC-CM2-SR5, CMCC-ESM2, MPI-ESM1-2-LR, NorESM2-LM, UKESM1-0-LL, and MIROC-ES2L, respectively). As a result, the net land nitrogen flux is mainly controlled by the organic nitrogen dynamics and shows consistency for the results from MAGICC emulation and ESM simulation (Fig. 3 and Fig. A4).

https://doi.org/10.5194/egusphere-2024-1941
Preprint. Discussion started: 18 September 2024

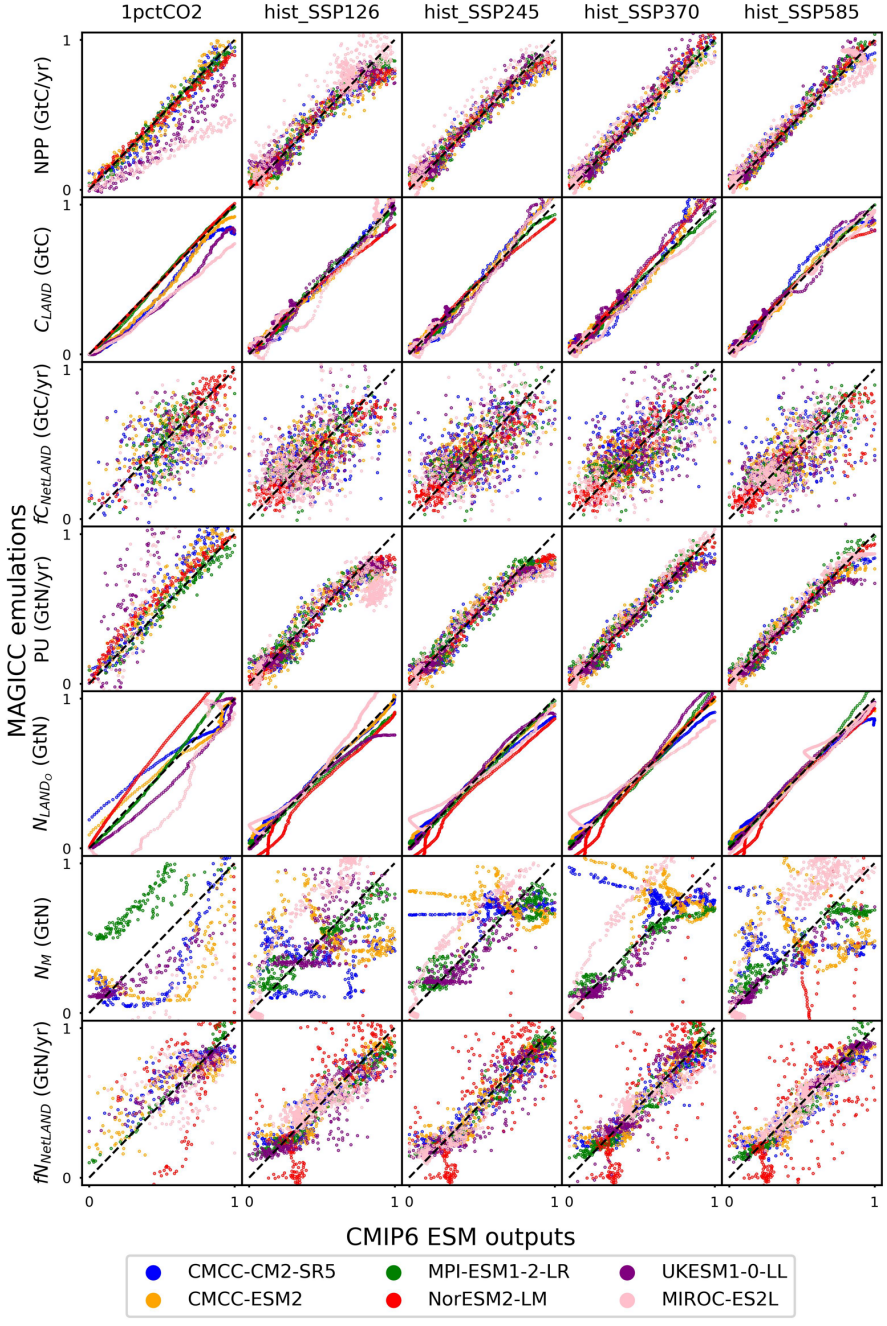

Figure 3. Comparison of net primary production (NPP), land carbon pool size (C_{LAND}), net land carbon flux ($fC_{NetLAND}$), nitrogen plant uptake (PU), land organic nitrogen pool size (N_{LANDo}, sum of nitrogen in plant, litter, and soil pools), mineral nitrogen pool size (N_M), and net land nitrogen flux ($fN_{NetLAND}$) between CMIP6 ESM outputs and MAGICC emulations. The results are scaled using the (max-min) calculated from CMIP6 ESM outputs, which are the target of the calibration. Diagonal dashed lines represented points where the emulation equals the target. Positions below/above the dashed lines indicate under-/over-estimation by the emulator.

https://doi.org/10.5194/egusphere-2024-1941
Preprint. Discussion started: 18 September 2024

4 Discussions

4.1 The climate and carbon-nitrogen cycle in CMIP6 ESMs

The climate and carbon-nitrogen cycle in CMIP6 ESMs remain considerably different (Fig. 4, Fig. A5, and Text A1), which contributes to the imperfect emulation (especially the mineral nitrogen pool size, Fig. 3). The following discussion of the ESM outputs provide an overview of the current model-based understanding of the climate and carbon-nitrogen cycle from a global-mean, annual-mean perspective, from which we suggest future research needs. For the sake of comparison, the subsequent figures/discussions focus on the common experimental periods for scenarios and ESMs (e.g., 1850-2100 for the hist_SSPs). If not specified, the value and spread in the discussion are expressed as mean ± one standard deviation across ESMs.

As a start, different ESMs have different temperature responses, which has flow-on effects for the carbon cycle and nitrogen cycle (Fig. A3). Regardless of the absolute land carbon/nitrogen pool sizes (Fig. A6 and Text A2), the accumulation of land carbon/nitrogen during the same experimental period and their trends are considerably more similar (Fig. 4A and Fig. 4B). The accumulated land carbon storage is 472±201, 127±28, 164±50, 165±100, and 227±100 GtC for the 1pctCO2, hist_SSP126, hist_SSP245, hist_SSP370, and hist_SSP585 experiments, respectively. The corresponding land nitrogen accumulation is 3.04±4.65, 3.28±1.03, 3.92±1.33, 3.76±1.32, and 3.54±1.64 GtN. Generally, the land carbon and nitrogen accumulation are proportional to maintain the stoichiometric relationship between carbon and nitrogen (Fig. 4A and Fig. 4B, the mean values). However, the opposite trend of land carbon and nitrogen change is found in the two CMCC ESMs (compared to the other ESMs) in their 1pctCO2 runs, which explains the much larger spread of land organic nitrogen accumulation at the end of 1pctCO2 compared to the four hist_SSPs (Fig. 4B). Both the land carbon and nitrogen storage show larger spread in the 1pctCO2 experiment (without land use changes), which further highlights the model structure uncertainty. The higher spread of carbon and nitrogen storage in higher warming scenarios indicates the feedback uncertainty (Melnikova et al., 2021).

The continuous and fast depletion of mineral nitrogen is found in NorESM2-LM in the 1pctCO2 scenario, coinciding with the highest accumulation of organic nitrogen (Fig. 4C). There are contrasting trends in mineral nitrogen pool size changes among models across all scenarios (Fig. 4C), indicating a large discrepancy and very limited agreement about mineral nitrogen estimation among ESMs. Better understanding and proper representation of organic nitrogen decomposition (nitrogen mineralization) is key to narrow the gap (Thomas et al., 2015; Forsmark et al., 2020; Davies-Barnard et al., 2020).

https://doi.org/10.5194/egusphere-2024-1941
Preprint. Discussion started: 18 September 2024

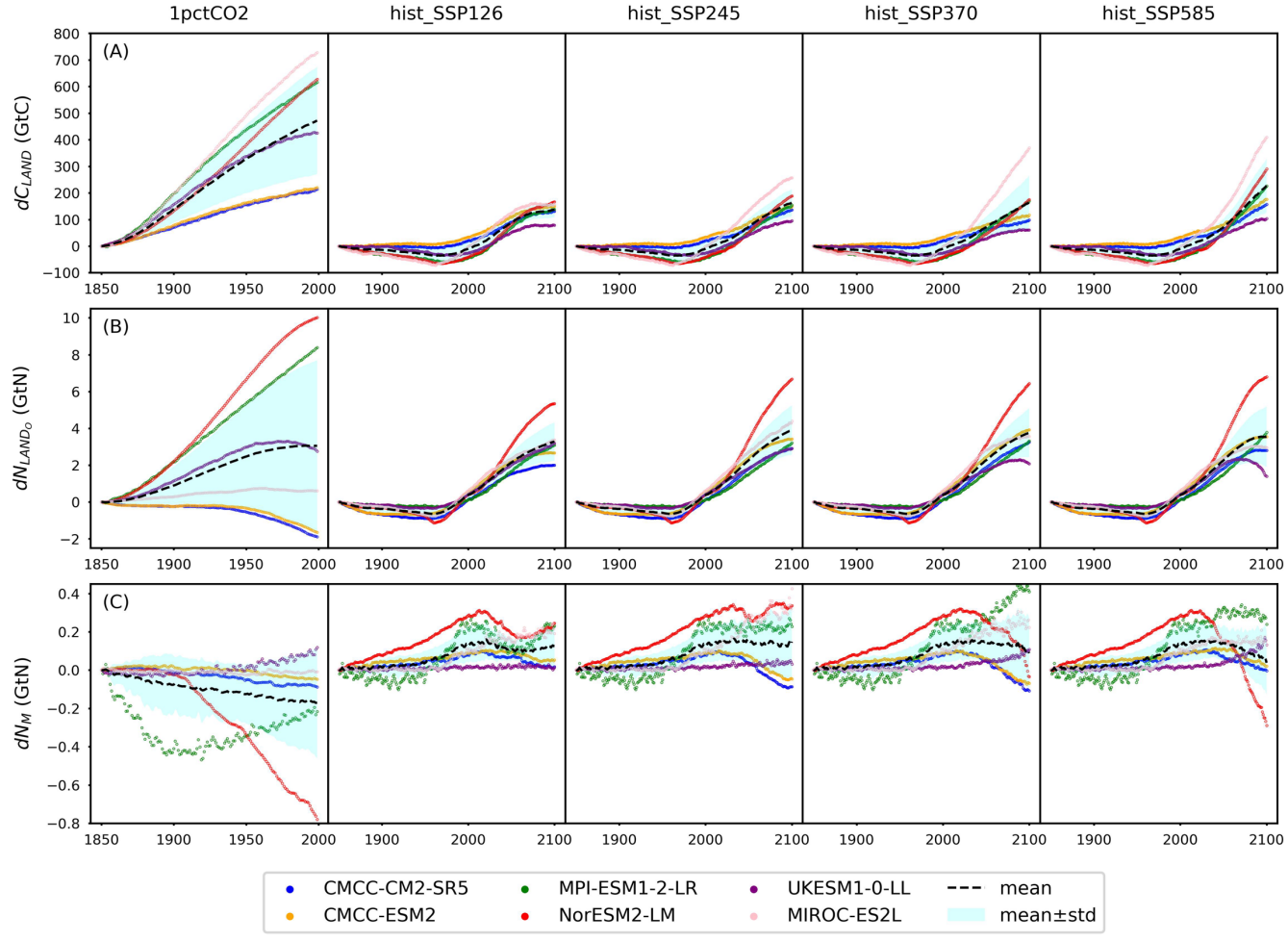

Figure 4. Carbon and nitrogen pool size dynamics [dC_{LAND}, delta land carbon pool size; dN_{LANDo}, delta land organic nitrogen pool size (sum of nitrogen in plant, litter, and soil pools); dN_M, delta mineral nitrogen pool size] from CMIP6 ESMs across different scenarios.

Because of the lack of observational constraints and process-level understanding, the terrestrial carbon cycle is a major source of uncertainty contributing to future climate projections and past climate simulations (Friedlingstein et al., 2014; Ciais et al., 2014). By analyzing outputs from 12 CMIP5 ESMs, a study has found that the projection uncertainty of global land carbon storage by 2100 is >160 GtC (more than 50% larger than that of the studied CMIP6 ESMs here), primarily driven by model structure differences (Lovenduski and Bonan, 2017). Though ESMs have been significantly improved over the past years (e.g., see Human Influence on the Climate System. In Climate Change 2021: The Physical Science Basis) (Eyring et al., 2019; Washington et al., 2009) - with the inclusion of a nitrogen cycle as a realistic constraint on the carbon cycle being the most recent (at the time of CMIP6) (Davies-Barnard et al., 2020; Wei et al., 2022), the spread of carbon-concentration feedback is not much narrowed from CMIP5 to CMIP6 (Arora et al., 2020). The variability in nitrogen pool size dynamics (Fig. 4B and Fig. 4C) indicates considerable nitrogen-related uncertainties accompanied with the carbon-nitrogen coupling

https://doi.org/10.5194/egusphere-2024-1941
Preprint. Discussion started: 18 September 2024

(Du et al., 2018; Thomas et al., 2015; Thomas et al., 2013). So far, there is no standardized nitrogen cycle validation for ESMs, largely because of limited observations, diverging representations, and the diverse upscaling approaches used in CMIP6 ESMs (Zaehle et al., 2014; Zaehle and Dalmonech, 2011; Spafford and Macdougall, 2021; Zhu et al., 2018). An improved quantification of nitrogen effects on the carbon cycle and climate, e.g., isolating the nitrogen cycle feedback from the carbon cycle feedback, though requiring meticulous experiment design and extra model simulation, might be necessary to improve climate projection uncertainty attribution (Spafford and Macdougall, 2021). The lack of nitrogen observations and limited mechanistic understanding remain a fundamental challenge in reducing uncertainty related to the nitrogen effect (Zaehle et al., 2014). The forthcoming online calibration of the updated MAGICC to CMIP6 ESMs and its application (e.g., sensitivity analyses, perturbed parameter analyses, and feedback analysis) should provide new insights into the projection uncertainty which would be too computationally expensive to obtain from ESMs (Hajima et al., 2020; Lawrence et al., 2019).

4.2 The nitrogen effect on NPP

The NPP simulated by CMIP6 ESMs has a consistent trend and is much more constrained than the pool sizes (Fig. 5A and Fig. A6). The NPP simulation in CMIP6 ESMs has been improved from the CMIP5 ESMs (Wei et al., 2022), attributed to advancements in nitrogen processes and the availability of more observational data (Collier et al., 2018; Randerson et al., 2009). Based on our calibrations, there is generally nitrogen limitation on global-mean, annual-mean NPP (Fig. 5B), which is consistent with experimental studies and other model simulations (Lebauer and Treseder, 2008; Wieder et al., 2015b; Thornton et al., 2009; Thornton et al., 2007). According to our calibrations, NorESM2-LM is the only model that shows nitrogen fertilization effects on NPP during the historical period, alongside a persistent intensification of nitrogen limitation during the scenario period. This historical fertilization coincides with an enrichment of the model's mineral nitrogen pool, while the increasing limitation correlates with the accumulation of organic nitrogen (see Fig. 4B, Fig. 4C, and Fig. A6D). These findings suggest that nitrogen mineralization is constrained by nitrogen availability during the scenario period in NorESM2-LM, resulting in reduced mineral nitrogen levels and thereby exacerbating NPP limitation.

Based on our calibrations, MPI-ESM1-2-LR and UKESM1-0-LL show the strongest nitrogen limitation on NPP during their hist_SSPs runs, with an $\epsilon_{CN(NPP)}$ range of 0.73-0.88 and 0.77-0.90, respectively. The strong nitrogen limitation from MPI-ESM1-2-LR in its 1pctCO2 simulation matches the continuous depletion of its mineral nitrogen pool (Fig. 4C). It is noted that JSBACH, the land component of MPI-ESM1-2-LR (Mauritsen et al., 2019), shows very limited nitrogen limitation on NPP in its CMIP5 1pctCO2 idealized simulation (Goll et al., 2017). The relatively more severe depletion of mineral nitrogen in its CMIP6 output (maximum >0.43 GtN, Fig. 4C) than its CMIP5 result (maximum <0.3 GtN, value from the reference publication), along with the much higher NPP simulated in CMIP6 (maximum ~110 GtC/yr, Fig. 5A) than CMIP5 (maximum ~40 GtC/yr, value from the reference publication), might be the reason for the strong nitrogen limitation. On the other hand, we suspect that the strong nitrogen limitation on NPP inferred for UKESM1-0-LL, is primarily the result of the incongruent high NPP and low plant uptake results from UKESM1-0-LL outputs (Fig. A4).

https://doi.org/10.5194/egusphere-2024-1941
Preprint. Discussion started: 18 September 2024

Based on our calibration, CMCC-CM2-SR5 and CMCC-ESM2 exhibit the least pronounced nitrogen limitation (or even fertilization) on NPP during their hist_SSPs runs, with an $\epsilon_{CN(NPP)}$ range of 0.93-1.05 and 0.93-1.03, respectively. The similarly weak limitation is also observed in our calibration to their 1pctCO2 runs. Their organic nitrogen pool sizes keep decreasing in the 1pctCO2 experiment (Fig. 4B and Fig. A6B), which should contribute a large flux of mineral nitrogen via decomposition. However, their mineral nitrogen pools are not enriched (Fig. A4 and Fig. A6D), indicating a considerable mineral nitrogen loss from these two models. The slight nitrogen fertilization on NPP ($\epsilon_{CN(NPP)} > 1$) is found in our calibration to the CMCC models from 1975 to 2025 or 2100 depending on the scenarios. The Community Land Model (CLM) serves as the land component for both CMCC models (Lovato et al., 2022). In the Duke and Oak Ridge National Laboratory (ORNL) Free-Air CO_2 Enrichment (FACE) experiments, CLM has exhibited a nearly negligible initial-year nitrogen-based NPP response (defined as NPP / canopy nitrogen), alongside a 6-10% NPP response to elevated CO_2 (Zaehle et al., 2014). The near-zero nitrogen-based NPP response and significant NPP increase suggest that CLM perceives a relatively high canopy nitrogen content (as supported by the large land organic nitrogen pool sizes in CMCC models' output in Fig. A6B). This potentially contributes to the weak nitrogen limitation observed in the CMCC models at the global scale and underscores the potential utility of regional observation studies to constrain the global nitrogen effect. Most nitrogen limitation factors fall within the range of 0.85-1.0, with limitations increasing in higher scenarios. This finding aligns with the OCN results from the RCP85 and RCP26 simulations (Fig. 2 and (Meyerholt et al., 2020)).

Although both land surface models and our calibrations to ESMs indicate a continuous nitrogen limitation on NPP at the global scale, there is room for debate regarding the realism of a long-term nitrogen limitation. Considering the substantial amounts of atmospheric nitrogen deposition and anthropogenic additions, alongside the ubiquitous presence of nitrogen-fixing organisms, the ability of ecosystems to optimize nitrogen use efficiency in response to varying nitrogen availability remains unclear. Previous studies suggest that ecosystems should be capable of effectively balancing these factors to alleviate long-term limitations on overall NPP (Vitousek and Howarth, 1991). This holds particularly true for tropical forests where nitrogen is abundant and rapidly circulated (Hedin et al., 2005; Cusack et al., 2011). In such cases, other nutrients like phosphorus and potassium might play a critical role (Wright et al., 2011; Alvarez-Clare et al., 2013). Further validation is required to assess the long-term effects of nitrogen limitation on NPP and to understand the differences between regional and global patterns.

https://doi.org/10.5194/egusphere-2024-1941
Preprint. Discussion started: 18 September 2024

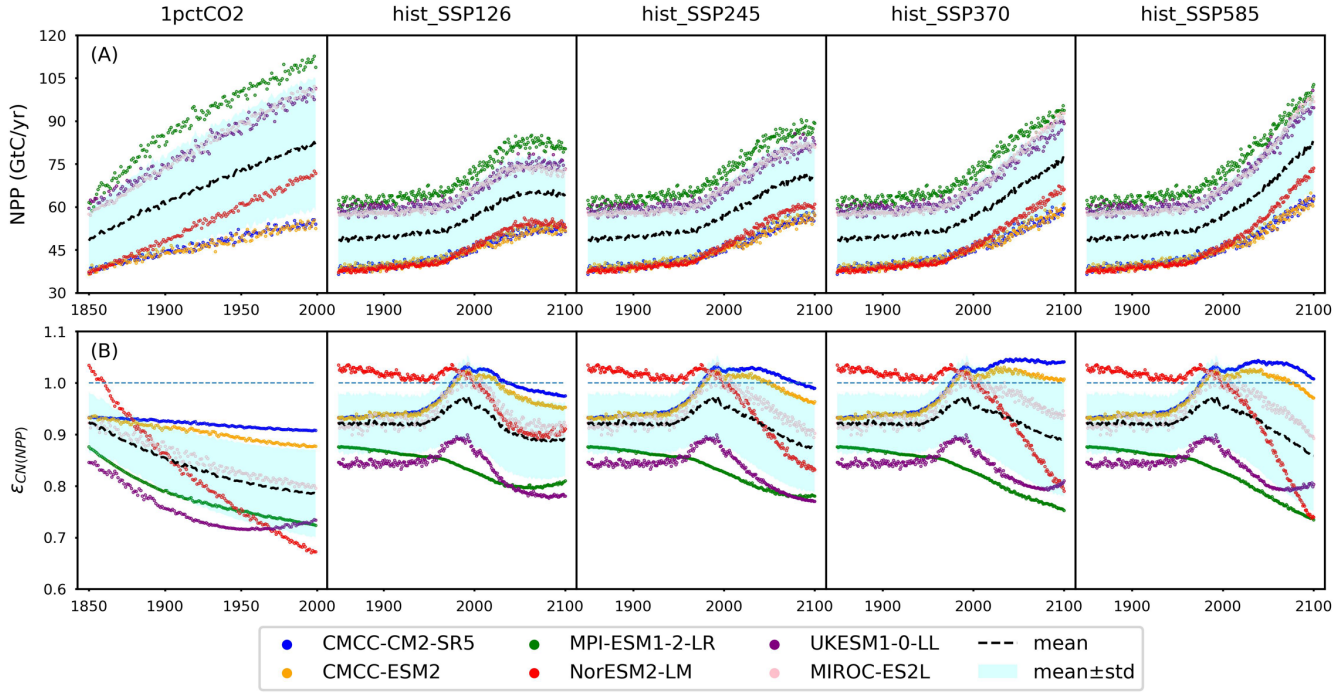

Figure 5. Net primary production (NPP) from CMIP6 ESMs and the emulated nitrogen effect on NPP ($\epsilon_{CN(NPP)}$) across different scenarios (The blue dashed line serves as a reference for $\epsilon_{CN(NPP)} = 1$)

4.3 The nitrogen effect on pool turnovers

According to our calibrations, the carbon-nitrogen coupling has largely enhanced plant carbon turnover in both CMCC models and MIROC-ES2L, as evidenced by $\epsilon_{CN(LP_c)}$ values ranging from 1.09 to 1.50, 1.07 to 1.50, and 1.12 to 1.40 respectively, during the hist_SSP period (Fig. 6A). The $\epsilon_{CN(LP_c)}$ values exhibit an increasing trend from the SSP126 scenario to the SSP585 scenario. The calibration to the other ESMs, however, suggest that the plant nitrogen status has inhibited litter production ($\epsilon_{CN(LP_c)}$ in the range of 0.6-0.8 during the hist_SSP period and no significant difference among different scenarios). The carbon-nitrogen coupling effect (ϵ_{CN}) and temperature effect (ϵ_{dT}) effectively change the turnover rate determined by the initial turnover times (Eqs. 30-36). Considering that the temperature feedback is always 1 at the beginning of each experiment (dT = 0) and the dynamics of plant carbon are similar across different ESMs (Fig. 4A and Fig. A4), the strong nitrogen enhancement on litter carbon production in the CMCC models is mainly because of their high initial plant carbon turnover times (31 and 66 years, respectively, Table A1), compared to the other ESMs (15 to 25 years, Table A1). The combination allows for the total litter production rate to remain at a similar level for all the ESMs, a key requirement given that they have similar plant pool size changes (Fig. A4), relatively consistent NPP (the influx for plant carbon pool, Fig. 5), and similar plant-litter respiration (the outflux for plant carbon pool, the LPR_0 parameter in Table A1). The enhanced litter production in MIROC-ES2L, however, is needed to compensate for its much lower plant respiration flux (LPR_0 = 0.96

https://doi.org/10.5194/egusphere-2024-1941
Preprint. Discussion started: 18 September 2024

GtC/yr in MIROC-ES2L vs. 4.16-9.90 GtC/yr in other ESMs). The weak limitation (or even fertilization) of NPP found for the CMCC models (Fig. 5B) and the continuous loss of soil organic nitrogen (Fig. 4B and Fig. A4, 1pctCO2 and historical period) suggest that the system is relatively less nitrogen limited. The resulting plant nitrogen availability partially contributes to the fast plant carbon turnovers in our calibration to the CMCC models.

Our calibrations to all the ESMs except for MPI-ESM1-2-LR show consistently inhibited litter decomposition after the nitrogen effect is applied ($\epsilon_{CN(LD_c)}$ in the range of 0.55-0.96 for the hist_SSP runs) and such inhibition slightly increases from SSP126 to SSP585. The significantly enhanced litter decomposition in our calibration to MPI-ESM1-2-LR is attributed to the high carbon input into its litter pool and the small temperature sensitivity, which are supported by 1) the highest NPP and its partition into the litter pool among the ESMs (Fig. 5A and Table A1, f_{NPP2L} = 0.59); 2) the highest litter production partition into litter pool (f_{LP2L_c} = 0.96, Table A1); and 3) the lowest temperature sensitivity of litter decomposition ($s_{dT(LD_c)}$ = 0.024, Table A1). The strong nitrogen limitation on NPP (Fig. 5B), the continuous depletion of the mineral nitrogen pool (Fig. 4C and Fig. A4, 1pctCO2 and historical period), and the highest biological nitrogen fixation (Fig. 7A) in our calibration to MPI-ESM1-2-LR indicates that the plant nitrogen is insufficient. The high $\epsilon_{CN(LD_c)}$ along with the low f_{LD2S_c} (0.07, Table A1) suggest that the system is trying to mineralize more litter carbon to mediate the plant nitrogen deficiency and to maintain an ecologically reasonable carbon:nitrogen stoichiometry.

The soil respiration is found to be restricted in our calibration to UKESM1-0-LL ($\epsilon_{CN(SR_c)}$ = 0.61-0.69 during the hist_SSP period), while it is significantly enhanced in other ESMs. The strongest enhancement is found in the two CMCC models ($\epsilon_{CN(SR_c)}$ = 1.24-1.50 during the hist_SSP period), followed by NorESM2-LM ($\epsilon_{CN(SR_c)}$ = 1.20-1.36 during the hist_SSP period). The calibrations to these three models show longer soil carbon turnover times (283-476 years, Table A1) than the other ESMs. The order of magnitude larger mineral nitrogen pool size in NorESM2-LM than other ESMs (Fig. A6D) and the continuously growing mineral nitrogen and organic nitrogen pool sizes (Fig. 4C, hist_SSPs) support the enhanced soil organic matter decomposition. It is observed that the mineral nitrogen pool size exhibits a continuous decrease during NorESM2-LM's 1pctCO2 run and by the end of its SSP585 run (Fig. 4D and Fig. A4). Considering that plant uptake and net mineralization are the two major fluxes controlling the mineral nitrogen dynamics, this result suggests a potential threshold associated with climate or CO_2 concentration, limiting the net mineralization rate from matching the ongoing increase in plant uptake (Fig. A4). The high temperature change (Fig. A5) and its subsequent high temperature effect on respiration in UKESM1-0-LL could be responsible for the nitrogen-inhibited soil respiration. The substantial land carbon accumulation in MIROC-ES2L (Fig. 4A) requires less respiration, thus explaining the neglectable nitrogen effect on its soil respiration. The diverse impacts of nitrogen on soil carbon turnover align with existing experimental findings, which have demonstrated contrasting trends in nitrogen additions across various substrate decompositions (Averill and Waring, 2018; Hobbie, 2008). As a result, studies have suggested that the classic stoichiometric decomposition theory should be revised (Craine et al., 2007).

https://doi.org/10.5194/egusphere-2024-1941
Preprint. Discussion started: 18 September 2024

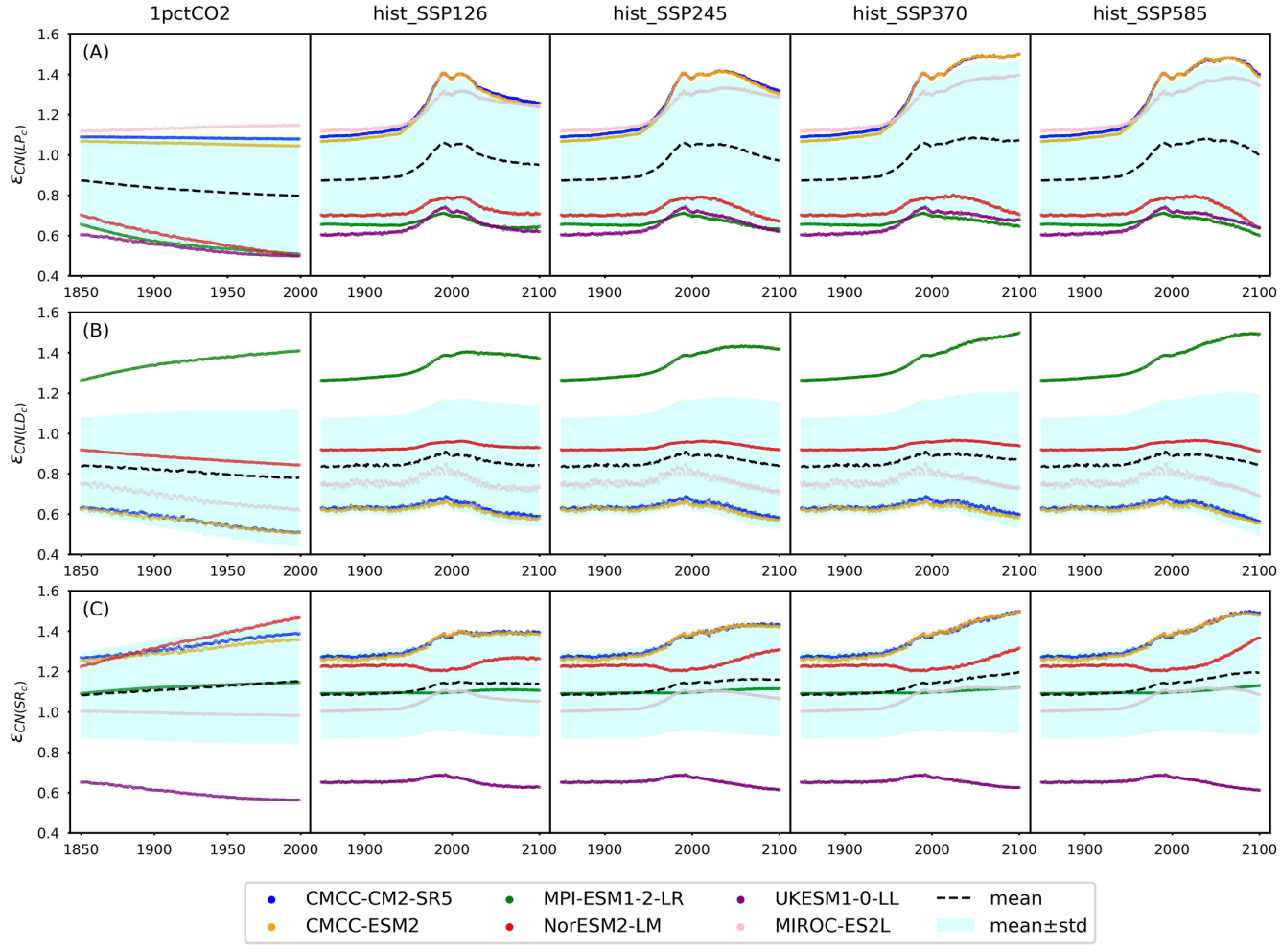

690 **Figure 6. The emulated nitrogen effect on carbon pool turnovers, including litter production ($\epsilon_{CN(LP_c)}$), litter decomposition ($\epsilon_{CN(LD_c)}$) and soil respiration ($\epsilon_{CN(SR_c)}$) from CMIP6 ESMs across different scenarios.**

5 Limitations and implications

5.1 The simulation of mineral nitrogen pool dynamics

Our emulation is less effective in capturing the mineral nitrogen pool sizes for some ESMs (e.g., NorESM2-LM, Fig. 3 and Fig. A4). However, the large mineral nitrogen pool in NorESM2-LM (Fig. A6D) and the large discrepancy of mineral
695 nitrogen pool size change among ESMs (Fig. 4C) and land surface models (Fig. 2) indicates that finding/applying more observational constraints/validation on the mineral pool size simulation from the complex models themselves, while challenging, should be a key focus (Zaehle and Dalmonech, 2011; Thomas et al., 2015). The heterogeneous terrestrial nitrogen cycle results in challenges and discrepancies even compared to the regional observations we do have (Schulte-

https://doi.org/10.5194/egusphere-2024-1941
Preprint. Discussion started: 18 September 2024

Uebbing and De Vries, 2018; Ramm et al., 2022; Menge et al., 2012). The uncertain atmospheric deposition and nitrogen fertilizer application further complicate the evaluation of the mineral nitrogen pool size and its dynamics (Mulvaney et al., 2009; Reay et al., 2008; Gruber and Galloway, 2008).

The two main controls of the mineral nitrogen pool size, the nitrogen mineralization (from organic decomposition) and mineral nitrogen loss, are still poorly understood at the process level (Manzoni et al., 2008; Hedin et al., 2005). For instance, the microbial decomposition of organic matter (heterotrophic respiration) can be limited, stimulated, or even unaffected by the nitrogen addition as a result of differences in soil microbial biomass or activity changes (Bardgett et al., 1999). The nitrogen effect on decomposition has been found to be sensitive to the types of substrates, but generally the impact on decomposition rate is negative or neutral (Hobbie, 2008). The root allocation, plant growth, litter production, biodiversity, etc., are all influenced by nitrogen (Phoenix et al., 2006; Wright et al., 2011). However, a 13-year-long nitrogen addition study has found that lower nitrogen addition rates had no effect on litter production or soil respiration in a Pinus sylvestris forest (Forsmark et al., 2020). This raises questions about the overall nitrogen effect at the ecosystem level, particularly considering the uneven geographical distribution of atmospheric nitrogen deposition (Phoenix et al., 2006). Alongside climate factors such as warming and precipitation, as well as other ecological or physical constraints, the situation becomes even more complicated (Plett et al., 2020; Lim et al., 2015; Cusack et al., 2010; Reich et al., 2014; Li et al., 2019). These findings underscore the highly complex dynamics of mineral nitrogen, suggesting that the current formulation of mineral nitrogen loss in MAGICC's nitrogen cycle, characterized by simple first-order decay and a single temperature response (Eq. 36), is very likely an oversimplification. Introducing constraints to the global stoichiometry of nitrogen mineralization could potentially enhance the modeling of mineral nitrogen pool dynamics (Manzoni et al., 2008; Meyerholt and Zaehle, 2015). Nevertheless, these new developments in MAGICC are a step towards better representation of carbon-nitrogen dynamics. The calibration results also demonstrate that the current MAGICC formulation mostly captures the trend of mineral nitrogen pool sizes in the majority of the studied CMIP6 ESMs and experiments (Fig. 3 and Fig. A4).

5.2 The biological nitrogen fixation as an input instead of being simulated

Biological nitrogen fixation serves as the primary non-anthropogenic nitrogen input in the global nitrogen cycle (Vitousek et al., 2002; Gruber and Galloway, 2008; Fowler et al., 2013). The trend of biological nitrogen fixation generally mirrors that of NPP (Fig. 7A and Fig. 5A), but the relative differences between ESMs are more pronounced (e.g., the largest initial biological nitrogen fixation found in MPI-ESM1-2-LR is approximately four times that of the smallest one found in NorESM2-LM). This similarity in trend arises because the model representations of biological nitrogen fixation in all the studied ESMs were based, at least partly, on its empirical relationship with either NPP or evapotranspiration derived from the widely recognized global biological nitrogen fixation estimate (Cleveland et al., 1999). Fig. 7B illustrates a variety of global patterns of biological nitrogen fixation/NPP in the CMIP6 ESM outputs, showcasing diverse trends such as decreases (CMCC-CM2-SR5, CMCC-ESM2, and MIROC-ES2L in the 1pctCO2 experiment), increases (UKESM1-0-LL in the 1pctCO2 experiment and MIROC-ES2L in SSP experiments), stability (UKESM1-0-LL in SSP scenarios), or even a peak

https://doi.org/10.5194/egusphere-2024-1941
Preprint. Discussion started: 18 September 2024

followed by a decrease (NorESM2-LM and MIROC-ES2L in high SSP scenarios). It is noteworthy that the mean biological nitrogen fixation/NPP remains relatively constant at approximately 0.0018 GtN/GtC across all experiments.

Recent findings from a meta-analysis of field measurements challenge the notion of a statistically significant relationship between biological nitrogen fixation and NPP/evapotranspiration (Davies-Barnard and Friedlingstein, 2020). An analysis of model uncertainty in recent studies highlighted that variations in the representation of biological nitrogen fixation could significantly impact future climate projections (Wieder et al., 2015a; Kou-Giesbrecht and Arora, 2022). For instance, employing different biological nitrogen fixation representations within a shared framework has resulted in modeled biological nitrogen fixation responses to elevated (200 ppm higher) CO_2 ranging from -4 to 56 $\times 10^{-3}$ GtN/yr. This variation has led to a global land carbon storage range of 281 to 353 GtC (over ~150 years of simulation), with N2O emissions fluctuating from -1.6 to 0.5 $\times 10^{-3}$ GtN/yr (Meyerholt et al., 2016). A recent study assessing biological nitrogen fixation structural uncertainty in CMIP6 ESMs has revealed that the response of biological nitrogen fixation and other nitrogen cycle variables could differ, even among models with similar structures (Davies-Barnard et al., 2022). Conflicting empirical relationships and updated observations underscore the considerable uncertainty and potential need for revisions to biological nitrogen fixation formulations in ESMs. While we could develop parameterizations to emulate the biological nitrogen fixation formulations used in ESMs, the biological nitrogen fixation flux represents a relatively minor flux with questionable data quality and highly uncertain formulations and/or mechanisms. Therefore, we opt not to pursue it further here. Instead, the current carbon-nitrogen cycle in MAGICC directly prescribes biological nitrogen fixation from CMIP6 ESM outputs to circumvent further structural uncertainty stemming from simplified parameterization.

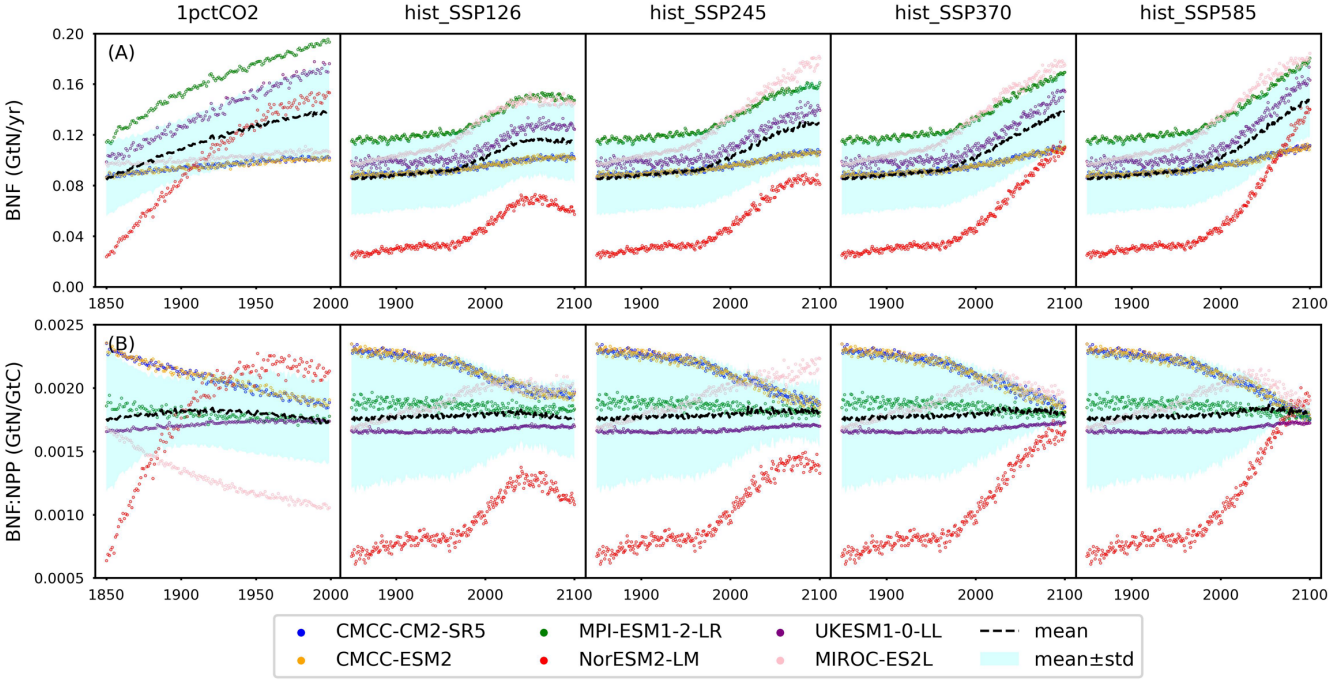

https://doi.org/10.5194/egusphere-2024-1941
Preprint. Discussion started: 18 September 2024

Figure 7. Biological nitrogen fixation (BNF) and its ratio to net primary production (BNF:NPP) from CMIP6 ESMs across different scenarios.

5.3 The disentangled climate feedback and nitrogen effect from emulation

One advantage of RCMs is that their simplified formulations attempt to capture the overall effects of complex processes in ESMs, aiding the identification and quantification of key effects in the system. Based on the assumptions and definitions in this updated carbon-nitrogen cycle, we can separate the temperature feedback and carbon-nitrogen coupling feedback for different pool turnovers (Eqs. 30-36). However, a significant challenge in this separation arises from the exponential formulation of both feedbacks and the increasing trends of all the feedback proxies (change in temperature (dT), nitrogen plant uptake (PU), and atmospheric deposition (AD), Fig. A3 and Fig. A4). This setup suggests that these feedbacks (or the related sensitivity parameters) may change in opposite directions to compensate each other while still producing a similar overall feedback. The formulations (Eqs.30-36) suggest that the turnover time and the overall feedback can also offset each other to reach a similar turnover flux.

To examine the correlation of parameter values and feedback separation, we applied Markov chain Monte Carlo (MCMC) sampling for the sensitivity parameters and turnover times for each of the individual ESMs. The results show that there is a weak-to-moderate negative correlation between temperature sensitivity and plant uptake sensitivity for most of the ESMs (the absolute value of Spearman's r = 0.04-0.72 for most cases, highlighted in yellow in Fig. A7). The strongest correlations are found in NorESM2-LM (Spearman's r = -0.53, -0.72, and -0.46 for the litter production, litter decomposition and soil respiration, respectively). The weakest correlations are found in MIROC-ES2L (Spearman's r = -0.04, -0.34, and 0.04 for the litter production, litter decomposition and soil respiration, respectively). The temperature sensitivity and atmospheric deposition sensitivity show relatively weak correlations (the absolute value of Spearman's $r < 0.3$ for most cases, Fig. A7).

The weak-to-moderate correlations between temperature sensitivity and plant uptake sensitivity are mainly due to the feedback proxies, change in temperature (dT) and plant uptake (PU), which, though both exhibiting the same increasing trend, do not strictly change with the same gradients (e.g., the temperature change fluctuates near zero while plant uptake shows a clear increasing trend from 1850-1975 in the historical simulations, Fig. A3 and Fig. A4). Increasing one sensitivity while decreasing another, though it could lead to similar overall feedback at the early stage when temperature change and plant uptake are less perturbed, cannot guarantee similar overall feedback throughout the entire time series (e.g., the difference of overall feedback from different sensitivities amplifies as the temperature change gets higher and plant uptake becomes larger). In other words, the parameter values cannot simply vary all toward the opposite direction to compensate for the feedback. Instead, to reach the desirable turnover flux to satisfy the pool size dynamics, the parameter values need to be adjusted (not necessarily offset each other) to obtain the respective "correct" or "best-estimate" feedback. Such results suggest that separating the carbon-nitrogen coupling feedback from the temperature feedback (the assumption for Eqs. 30-36) is a reasonable assumption, although this should be investigated further in future work.

https://doi.org/10.5194/egusphere-2024-1941
Preprint. Discussion started: 18 September 2024

The turnover times and plant uptake sensitivities exhibit strong positive correlations in all the ESMs (displayed in bold in Fig. A7), indicating that plant uptake sensitivity is the predominant factor influencing the overall feedback to compensate for turnover time changes. This is supported by the dominance of carbon-nitrogen coupling feedback in both the magnitudes and trends of the overall feedback (Fig. 6 and Fig. A8), further emphasizing the substantial disparity between temperature feedback and carbon-nitrogen coupling feedback, and the imperative of distinguishing the two.

One limitation of disentangling the carbon-nitrogen coupling feedback from the climate feedback is that the feedback strength is primarily derived from emulation. Although several factors support this distinction: 1) the evidence presented in Fig. A7 and Fig. A8 underscores the clear differentiation between climate feedback and carbon-nitrogen coupling feedback; 2) the dynamics of pool size offer indirect yet compelling constraints (referred to as "emergent" constraints) for the feedback; and 3) the selection of feedback formulations (exponential rather than linear relationships) and proxies (with varying magnitudes) further restricts the parameters from offsetting each other. However, the absence of nitrogen-off simulations from the CMIP6 ESMs presents challenges for direct verification. Given the computational expense of running all scenarios in nitrogen-off mode, it is recommended that ESMs perform nitrogen-off simulations for select idealized scenarios (e.g., 1pctCO2 or flat10) for diagnostic purposes.

It should be noted that the feedback, as well as the pool size dynamics and fluxes, discussed in this paper are aggregated from extensive spatiotemporal datasets into an annual and global domain. Consequently, the carbon-nitrogen cycle represents a synthesis of various regional and sub-annual dynamics. Therefore, the results presented here are at a global scale, which may differ from regional or sub-regional studies and therefore requires careful interpretation.

6 Conclusion and future work

In this work we have detailed a new carbon-nitrogen coupled model within the reduced complexity model, MAGICC. Based on the offline calibration results from land surface models and multiple CMIP6 ESMs, we have demonstrated that the new carbon-nitrogen cycle model is able to effectively emulate the behavior of the carbon-nitrogen cycles from various, more complex models, encompassing a broad spectrum of carbon-nitrogen states and dynamics.

The temperature change and carbon-nitrogen state/dynamics (especially those related to the nitrogen cycle and mineral nitrogen) exhibit significant variability among CMIP6 ESMs, particularly in their 1pctCO2 and high SSP scenario runs, which highlights the model structure uncertainty. The contrasting trends in mineral nitrogen dynamics and the magnitude of order differences in pool sizes underscore the limited agreement in mineral nitrogen modeling. A thorough analysis, focusing on the new uncertainties introduced by the nitrogen cycle is imperative for the CMIP6 and future ESMs. The upcoming (in future research) sensitivity analysis, perturbation parameter analysis, and feedback analysis of the updated MAGICC model are expected to provide insights for uncertainty attribution.

The MAGICC emulation indicates a general nitrogen limitation on NPP, which follows a similar trend across the studied CMIP6 ESMs. Combining the results from NPP and turnovers suggests that, at the multi-model mean level, the carbon-

https://doi.org/10.5194/egusphere-2024-1941
Preprint. Discussion started: 18 September 2024

nitrogen coupling limits both NPP and plant and litter carbon pool turnovers, though the weaker NPP nitrogen limitation could also lead to significantly enhanced litter production. Soil respiration is instead enhanced in most of the ESMs. The combination indicates that terrestrial ecosystems may become net carbon sources sooner than we would expect based on models that do not consider the impact of the nitrogen cycle.

The presented carbon-nitrogen coupling in MAGICC demonstrates the ability to emulate many complex models, while nonetheless having limitations, particularly in simulating mineral nitrogen pool dynamics and biological nitrogen fixation. There are currently significant inconsistencies between ESM outputs and observations of the mineral nitrogen pool size and biological nitrogen fixation, both in terms of magnitudes and trends, suggesting that substantial revisions are possible in the near future. Therefore, the current formulation and treatment of these aspects in MAGICC may have to be updated too, while aiming to continue to strike a balance between model simplicity and performance, reflecting a fundamental design principle for RCMs and MAGICC in particular. Future work on MAGICC's carbon-nitrogen cycle will involve the online calibration of the full MAGICC structure to CMIP6 ESMs, sensitivity analysis, probabilistic projection application, and further development of the model following updates of complex models and theories.

https://doi.org/10.5194/egusphere-2024-1941
Preprint. Discussion started: 18 September 2024

Appendix

Table A1. Full list of calibrated carbon-nitrogen cycle parameters.

Parameter	CMCC-CM2-SR5	CMCC-ESM2	MPI-ESM1-2-LR	NorESM2-LM	UKESM1-0-LL	MIROC-ES2L	CABLE	OCN
NPP_0	41.92	41.88	68.93	36.23	69.95	62.06	57.38	53.98
LPR_0	8.58	6.20	9.90	6.56	4.16	0.96	7.81	9.00
CO_{2ref}	284.317	284.317	284.317	284.317	284.317	284.317	296.474	285.24
CO_{2b}	31	31	31	31	31	31	31	31
$s_{CO_2}^{log}$	0.000	0.788	1.451	0.948	0.113	0.004	2.582	0.594
$s_{CO_2}^{sig}$	335.90	297.10	337.71	263.82	250.77	269.25	315.82	289.88
m_{CO_2}	1.82	2.00	0.53	0.01	0.99	2.00	0.00	1.00
$s_{dT(NPP)}^{exp}$	-0.293	0.108	-0.300	-0.121	-0.223	-0.016	-0.143	-0.156
$s_{dT(NPP)}^{sig}$	0.245	0.143	1.192	0.314	0.249	0.278	-0.147	0.512
m_{dT}	0.82	0.99	0.30	0.56	0.84	0.93	0.83	0.38
$s_{dT(LPR)}$	-0.25	-0.22	-0.12	0.16	-0.19	0.30	-0.10	0.06
$s_{dT(LP_c)}$	0.040	0.056	0.054	-0.124	0.040	-0.051	0.001	-0.061
$s_{dT(LD_c)}$	0.073	0.063	0.024	-0.028	/	0.032	0.045	-0.007
$s_{dT(SR_c)}$	0.043	0.045	0.046	-0.042	0.064	0.027	0.066	0.046
$s_{dT(PU)}$	-0.003	-0.013	0.011	0.015	-0.048	-0.019	0.014	0.008
PU_{max}	2.57	3.00	2.06	2.30	2.67	2.42	1.89	2.17
NPP_{ref}	49.45	55.91	48.21	41.78	118.97	107.90	54.17	40.79
$\epsilon_{CN(NPP)0}$	0.96	1.03	1.23	1.41	1.23	1.07	1.58	1.19
f_1	2.31	2.26	0.00	1.25	1.69	2.54	0.64	0.26
f_2	-0.09	-0.19	-0.33	-0.46	-0.84	-0.47	-0.80	-0.17
$s_{PU(LP_c)}$	-0.032	-0.078	-0.517	-0.562	-1.778	0.142	0.079	0.060
$s_{PU(LD_c)}$	-0.740	-0.759	0.222	-0.142	/	-1.009	-0.008	0.104
$s_{PU(SR_c)}$	0.309	0.288	0.098	0.299	-1.363	-0.113	-0.058	0.009
$s_{AD(LP_c)}$	5.716	6.354	3.095	3.929	6.884	3.015	0.304	-0.826
$s_{AD(LD_c)}$	3.925	3.738	1.453	1.235	/	4.438	0.417	-0.420
$s_{AD(SR_c)}$	0.833	1.158	-0.190	-1.236	3.092	2.355	0.043	0.026
φ	0.99	1.00	0.97	1.00	1.00	1.00	1.00	0.94
τ_{rgr}	96.00	73.02	149.00	149.18	50.05	93.51	52.72	107.39
f_{NPP2P}	0.62	0.38	0.36	0.63	0.49	0.66	0.95	0.54
f_{NPP2L}	0.20	0.36	0.59	0.35	/	0.20	0.03	0.41
f_{LP2L_c}	0.94	0.92	0.96	0.72	/	0.49	0.89	0.99
f_{LD2S_c}	0.01	0.11	0.07	0.07	/	0.97	0.02	0.00
f_{LU2P_c}	0.88	0.88	0.88	0.92	0.94	0.56	0.53	0.11

https://doi.org/10.5194/egusphere-2024-1941
Preprint. Discussion started: 18 September 2024

f_{LU2L_c}	0.00	0.04	0.10	0.05	/	0.30	0.09	0.84
τ_{C_P}	31.26	66.11	24.42	22.56	14.96	16.14	15.46	22.89
τ_{C_L}	1.30	1.35	7.40	1.15	99.99	7.72	4.09	6.98
τ_{C_S}	452.96	283.42	117.35	476.71	20.99	22.01	125.82	290.81
$s_{dT(LP_n)}$	0.011	-0.015	-0.051	-0.062	-0.010	-0.018	0.027	-0.031
$s_{dT(LD_n)}$	0.065	0.038	0.000	0.014	0.002	0.005	0.021	0.037
$s_{dT(SR_n)}$	0.014	0.011	0.010	0.005	0.049	0.028	0.056	0.007
$s_{dT(LS_n)}$	0.056	0.051	-0.005	0.299	0.012	0.042	-0.007	0.088
$s_{PU(LP_n)}$	-0.306	0.134	-0.724	0.600	-2.519	1.159	-0.896	0.583
$s_{PU(LD_n)}$	-1.029	-0.449	0.498	0.148	0.000	1.909	0.473	-0.661
$s_{PU(SR_n)}$	0.810	0.892	0.161	0.977	-1.047	1.041	-0.073	0.685
$s_{AD(LP_n)}$	2.282	0.791	4.425	2.845	6.632	1.790	0.188	-2.124
$s_{AD(LD_n)}$	2.504	1.205	0.955	0.224	0.001	-0.064	-0.052	-1.172
$s_{AD(SR_n)}$	-0.510	-0.777	-0.745	-0.844	2.294	1.851	-0.975	-0.401
f_{BNF2P}	0.00	0.05	0.32	0.13	0.13	0.15	0.73	0.23
f_{BNF2L}	0.01	0.17	0.48	0.02	/	0.21	0.04	0.25
f_{PU2P}	0.23	0.14	0.04	0.41	0.04	0.98	0.17	0.13
f_{PU2L}	0.74	0.34	0.82	0.06	/	0.01	0.72	0.00
f_{LP2L_n}	0.66	0.16	0.40	0.03	/	0.17	0.04	0.19
f_{LD2S_n}	0.77	0.46	0.01	0.78	/	0.88	0.37	0.89
f_{LU2P_n}	0.61	0.12	0.31	0.24	0.13	0.10	0.51	0.16
f_{LU2L_n}	0.33	0.13	0.30	0.41	/	0.28	0.39	0.25
τ_{N_P}	14.12	30.66	28.03	36.84	46.98	15.74	12.81	33.79
τ_{N_L}	0.61	2.20	6.81	10.85	1.02	670.15	3.03	14.23
τ_{N_S}	690.09	728.42	318.18	601.92	222.76	247.10	108.00	180.87
τ_{N_M}	6.49	6.73	11.46	58.17	0.92	1.37	1.99	0.44

https://doi.org/10.5194/egusphere-2024-1941
Preprint. Discussion started: 18 September 2024

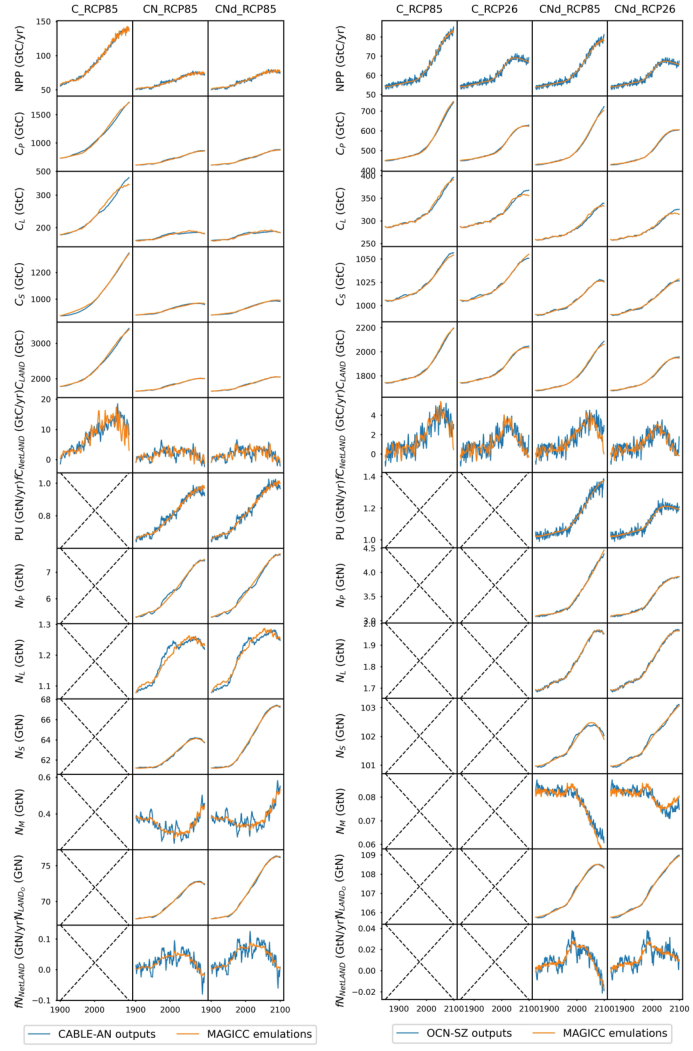

Figure A1. Comparison of net primary production (NPP), plant carbon pool size (C_P), litter carbon pool size (C_L), soil carbon pool size (C_S), land carbon pool size (C_{LAND}), net land carbon flux ($fC_{NetLAND}$), nitrogen plant uptake (PU), plant nitrogen pool size (N_P), litter nitrogen pool size (N_L), soil nitrogen pool size (N_S), mineral nitrogen pool size (N_M), land organic nitrogen pool size (N_{LANDo}, sum of nitrogen in plant, litter, and soil pools), and net land nitrogen flux ($fN_{NetLAND}$) between CABLE or OCN outputs (blue lines) and MAGICC emulations (orange lines). The experiments labeled as C, CN, and CNd denote the carbon-only, carbon-nitrogen coupled with constant nitrogen atmospheric deposition, and carbon-nitrogen coupled with dynamic nitrogen atmospheric deposition configurations in the land surface models, respectively.

https://doi.org/10.5194/egusphere-2024-1941
Preprint. Discussion started: 18 September 2024

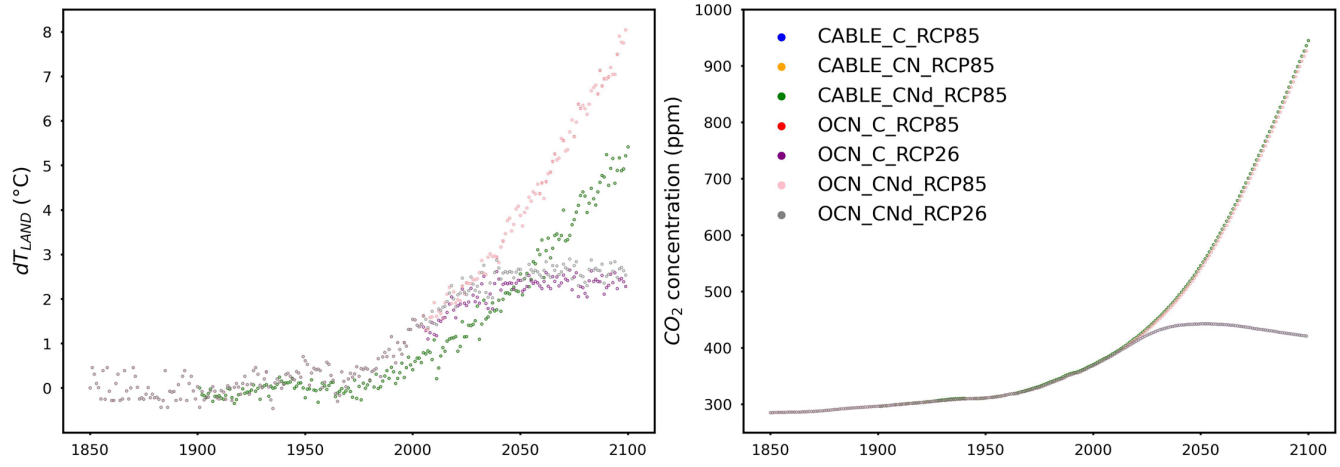

Figure A2. Global average surface temperature change over land (dT_{LAND}, delta annual mean tas over land) and CO_2 concentrations from land surface models across different scenarios.

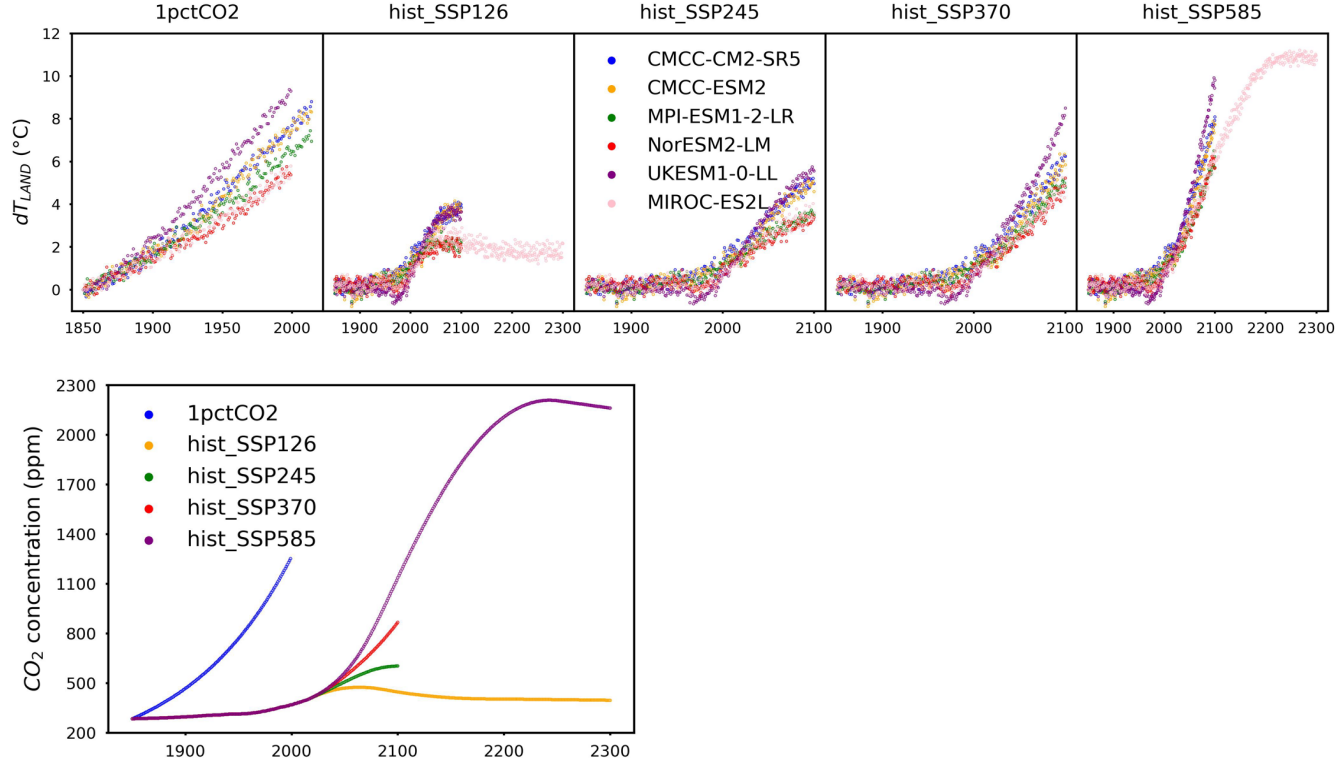

Figure A3. Global average surface temperature change over land (dT_{LAND}, delta annual mean tas over land) and CO_2 concentrations from CMIP6 ESMs across different scenarios.

https://doi.org/10.5194/egusphere-2024-1941
Preprint. Discussion started: 18 September 2024

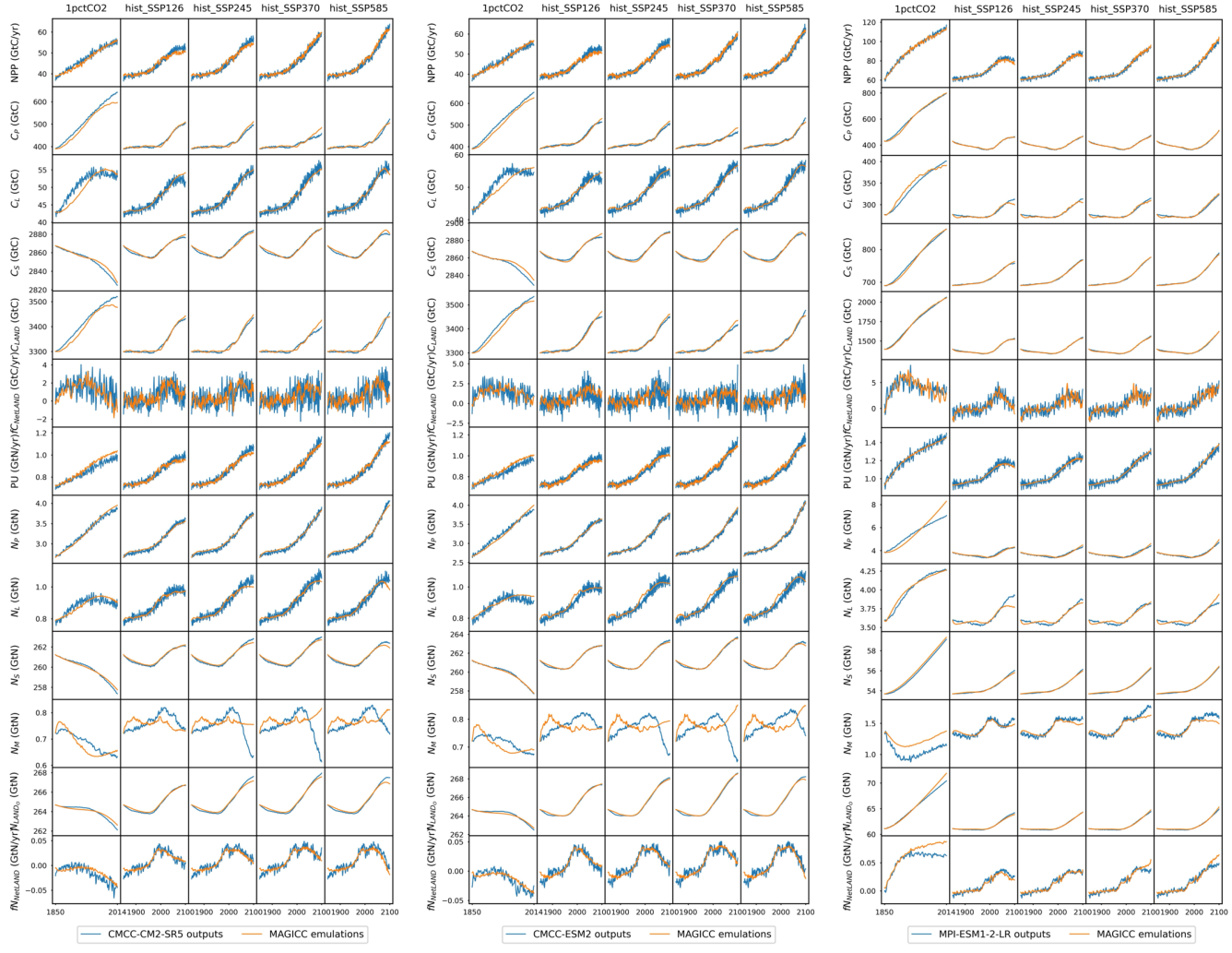

https://doi.org/10.5194/egusphere-2024-1941
Preprint. Discussion started: 18 September 2024

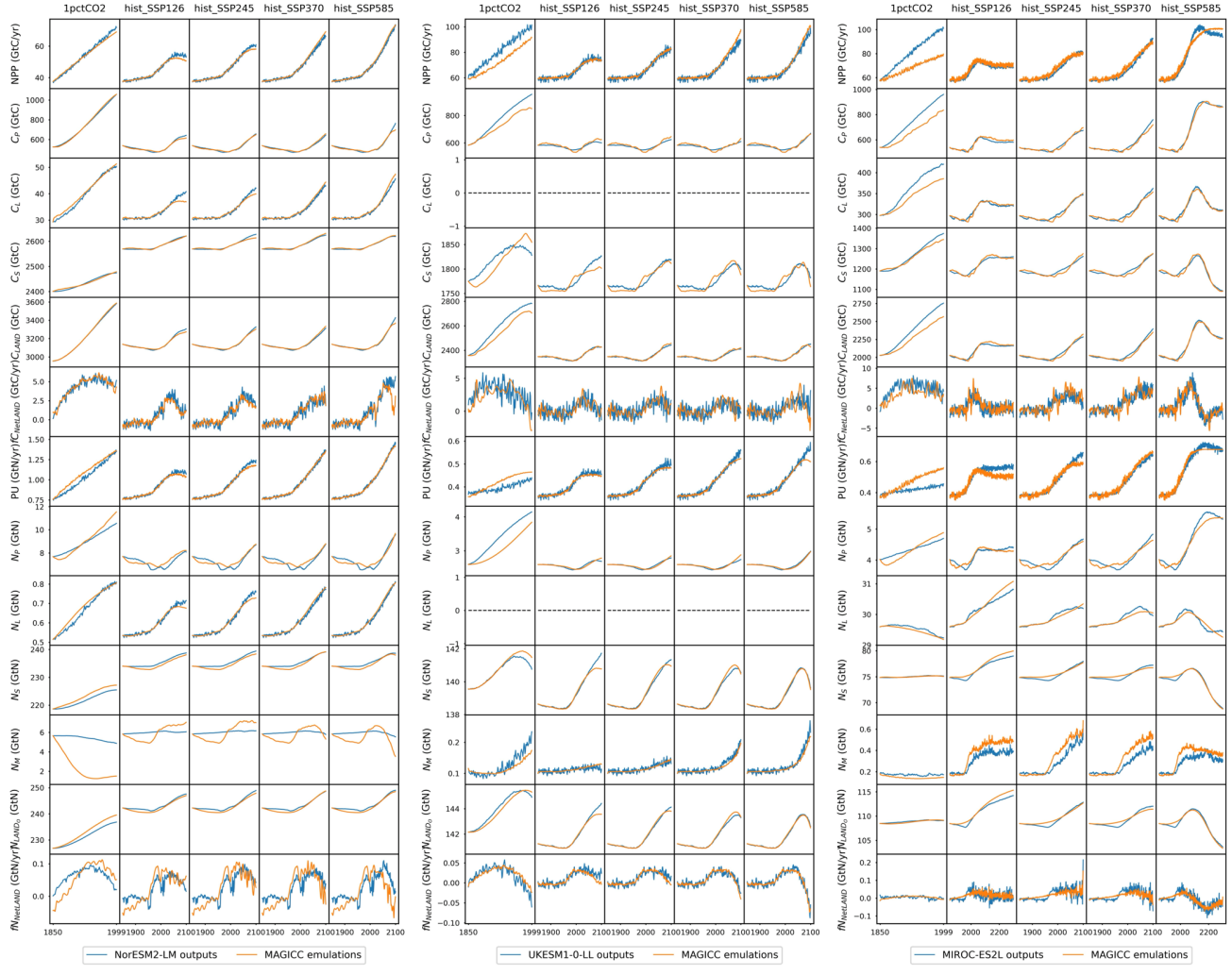

Figure A4. Comparison of net primary production (NPP), plant carbon pool size (C_P), litter carbon pool size (C_L), soil carbon pool size (C_S), land carbon pool size (C_{LAND}), net land carbon flux ($fC_{NetLAND}$), nitrogen plant uptake (PU), plant nitrogen pool size (N_P), litter nitrogen pool size (N_L), soil nitrogen pool size (N_S), mineral nitrogen pool size (N_M), land organic nitrogen pool size (N_{LANDo}, sum of nitrogen in plant, litter, and soil pools), and net land nitrogen flux ($fN_{NetLAND}$) between CMIP6 ESM outputs (blue lines) and MAGICC emulations (orange lines).

https://doi.org/10.5194/egusphere-2024-1941
Preprint. Discussion started: 18 September 2024

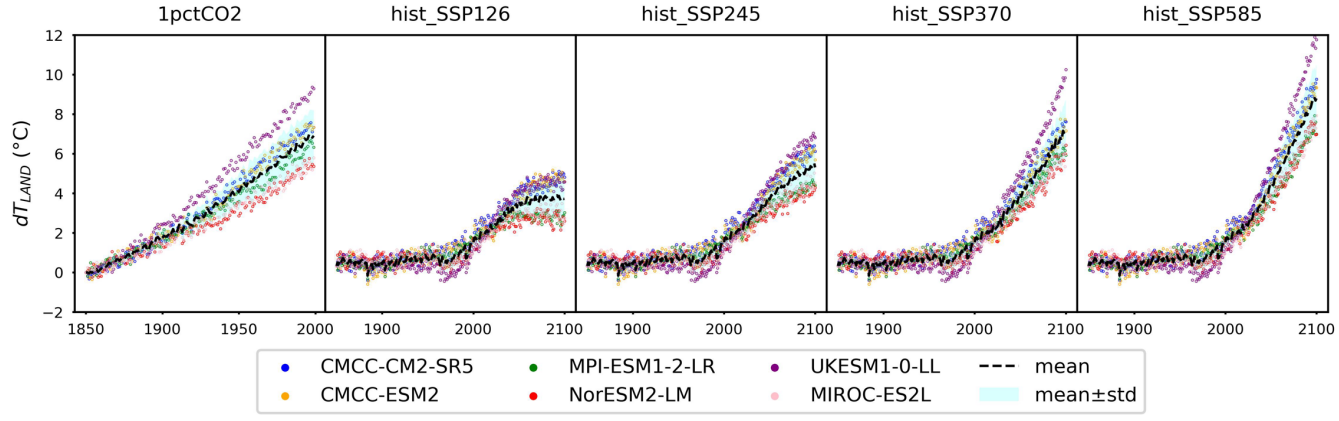

Figure A5. Global average surface temperature change over land (dT_{LAND}, delta annual mean tas over land) from CMIP6 ESMs across different scenarios (over the common experimental period).

Text A1. Supporting discussions on Figure A5

Temperature change, a pivotal driving force for the carbon-nitrogen cycle, exhibits significant variation between the two land surface models (Fig. A2) and among the simulations of CMIP6 ESMs (Fig. A3), even when they undergo the same experiment. For the sake of comparison, Fig. A5 and the subsequent discussions focus on the common experimental periods for scenarios (e.g., 1850-2100 for the hist_SSPs).

UKESM1-0-LL shows the highest temperature change among all models and experiments, whereas NorESM2-LM exhibits the lowest temperature change. Both the idealized 1pctCO2 - one of the base experiments in the Diagnostic, Evaluation and Characterization of Klima (DECK) experiments - and the historical simulation is in the core set of experiments performed under CMIP5, CMIP6, and previous CMIPs (Eyring et al., 2016; Taylor et al., 2012). As CMIP6 and C4MIP necessitate consistent forcings and experimental protocols for simulations conducted by participating ESMs (Eyring et al., 2016; Jones et al., 2016), the wide spread of the land surface temperature change - especially from the 1pctCO2 experiment where land use change is not included (with a standard deviation of 1.3°C and absolute difference of 3.9°C at the end of the simulation) - highlights the various parameterizations of physical processes in ESMs resulting in large differences of the ESMs climate sensitivities (Rugenstein et al., 2020; Meehl et al., 2020), for example, the structural uncertainty (Deser et al., 2020; Duan et al., 2021). The previous MAGICC simulation with constrains from historical CO_2 measurements and temperature observations is found reducing uncertainty in the temperature projections (Bodman et al., 2013).

Recent studies interpreting surface air temperature outputs from multiple CMIP6 ESMs indicate that the multi-model mean effectively captures the historical temperature trend in observations (Fan et al., 2020; Papalexiou et al., 2020). Results from a study using outputs from 29 CMIP6 ESMs show that the post-1988 warming is overestimated in 90% of the simulations and the observed long-term persistence of global mean temperature (for the period of 1880-2014) is not accurately captured in most of ESMs (Papalexiou et al., 2020), suggesting further model selections based on the case-specific indented uses. However, previous evaluation of the long-term persistence of temperature on continental areas (60°S-60°N) during 1930-

https://doi.org/10.5194/egusphere-2024-1941
Preprint. Discussion started: 18 September 2024

2004 in CMIP5 ESMs demonstrated that most models captured the long-term persistence reasonably well (Kumar et al., 2013). Moreover, grouping CMIP6 ESMs and re-analysing the global mean temperature based on the grouped models can also lead to different conclusions on the warming trend (Scafetta, 2023). These results indicate that more careful interpretation of the simulated temperature was needed. They also justified that using each ESM's global mean land temperature as input in this study instead of the global mean temperature is more reasonable (to avoid differences in calibration based on inconsistency with the target model's temperature rather than any issue with the reduced complexity model).

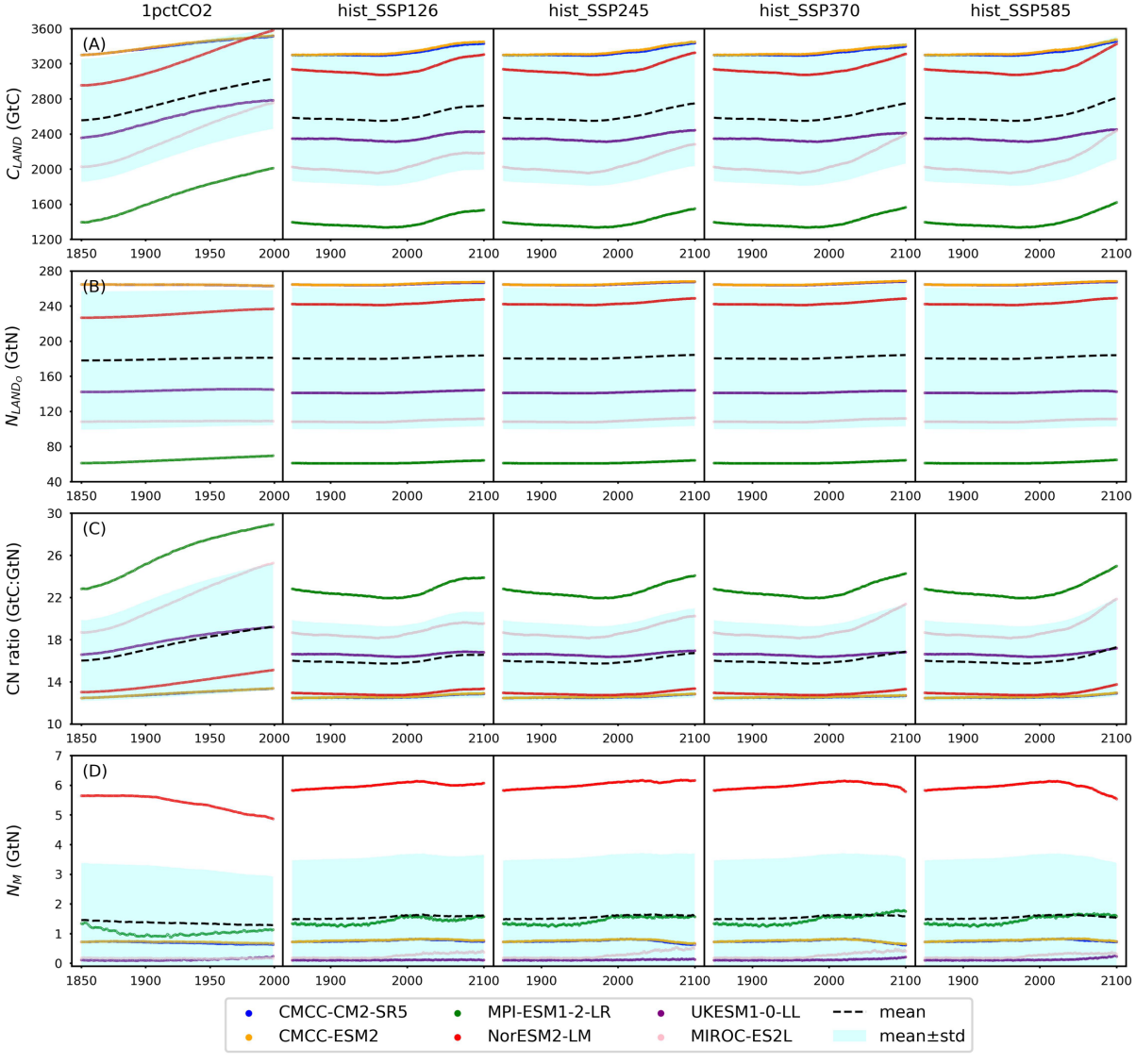

Figure A6. Diversity of land carbon pool size (C_{LAND}), land organic nitrogen pool size (N_{LANDo}, sum of nitrogen in plant, litter, and soil pools), carbon:nitrogen ratio (CN ratio), and mineral nitrogen pool size (N_M) from CMIP6 ESM outputs.

https://doi.org/10.5194/egusphere-2024-1941
Preprint. Discussion started: 18 September 2024

Text A2. Supporting discussions on Figure A6

Based on the varied temperature results, it is not surprising that the carbon-nitrogen cycle fluxes and pools from the CMIP6 ESMs are diverse (Fig. A6). The initial land carbon pool ranges from 1396 GtC (MPI-ESM1-2-LR) to notably higher values of 3300 GtC (CMCC-CM2-SR5 and CMCC-ESM2). The initial nitrogen pool sizes are even more inconsistent among ESMs. The largest initial organic nitrogen pool is 265 GtN from the two CMCC models, which is more than four times of the smallest one from MPI-ESM1-2-LR (61 GtN). These results have led to a wide range of initial organic carbon:nitrogen ratio from 12 (the two CMCC models) to 23 (MPI-ESM1-2-LR) (Fig. A6C). The trends for the carbon pool size, organic nitrogen pool size, and carbon:nitrogen ratio exhibit a similar pattern. They display a consistent increase in the 1pctCO2 scenario, while in the hist_SSP simulations, they initially decrease (1850-1970) and then rise again (1970-2100). The mineral nitrogen pool, on the contrary, shows significant variations in both pool sizes and trends across CMIP6 ESMs (Fig. A6D). The initial pool sizes range from <0.2 GtN (UKESM1-0-LL and MIROC-ES2L) to 5.6 GtN (NorESM2-LM). The trends are found either opposite or unrelated.

The substantial variation of simulated carbon pools is a long-standing issue for both CMIP5 and CMIP6 ESMs (Anav et al., 2013; Varney et al., 2022). The initial condition differences are responsible for the model's internal variability (Deser et al., 2020; Kumar and Ganguly, 2018), which accounts for more than half of the inter-model spread in near-term climate projections (Deser et al., 2012). Such differences also contribute to their respective carbon cycle projections. The different initial carbon-nitrogen cycle state among different ESMs further complicates their comparison (Spafford and Macdougall, 2021). The standard deviation of initial land carbon pool sizes is different for the 1pctCO2 (699 GtC) and historical (720 GtC) scenarios. Four of the studied ESMs have used nearly the same starting land carbon pool size for both scenarios (difference <1.5 GtC) while UKESM1-0-LL and NorESM2-LM have a large difference of 9 GtC and 184 GtC (out of a total of roughly 2300 GtC in UKESM1-0-LL and 3000 GtC in NorESM2-LM), respectively. The varying initial pool sizes can pose significant challenges for emulators employing first-order decay for pool turnovers, as the turnover time predominantly influences the magnitude of the "base" turnover flux (e.g., without any feedback scalers). Since MAGICC emulation has used the same set of parameters (including the turnover times) to emulate all the experiments, it explains the jump of the emulated soil carbon pool sizes in the 1pctCO2 experiment for these two models (Fig. A4).

https://doi.org/10.5194/egusphere-2024-1941
Preprint. Discussion started: 18 September 2024

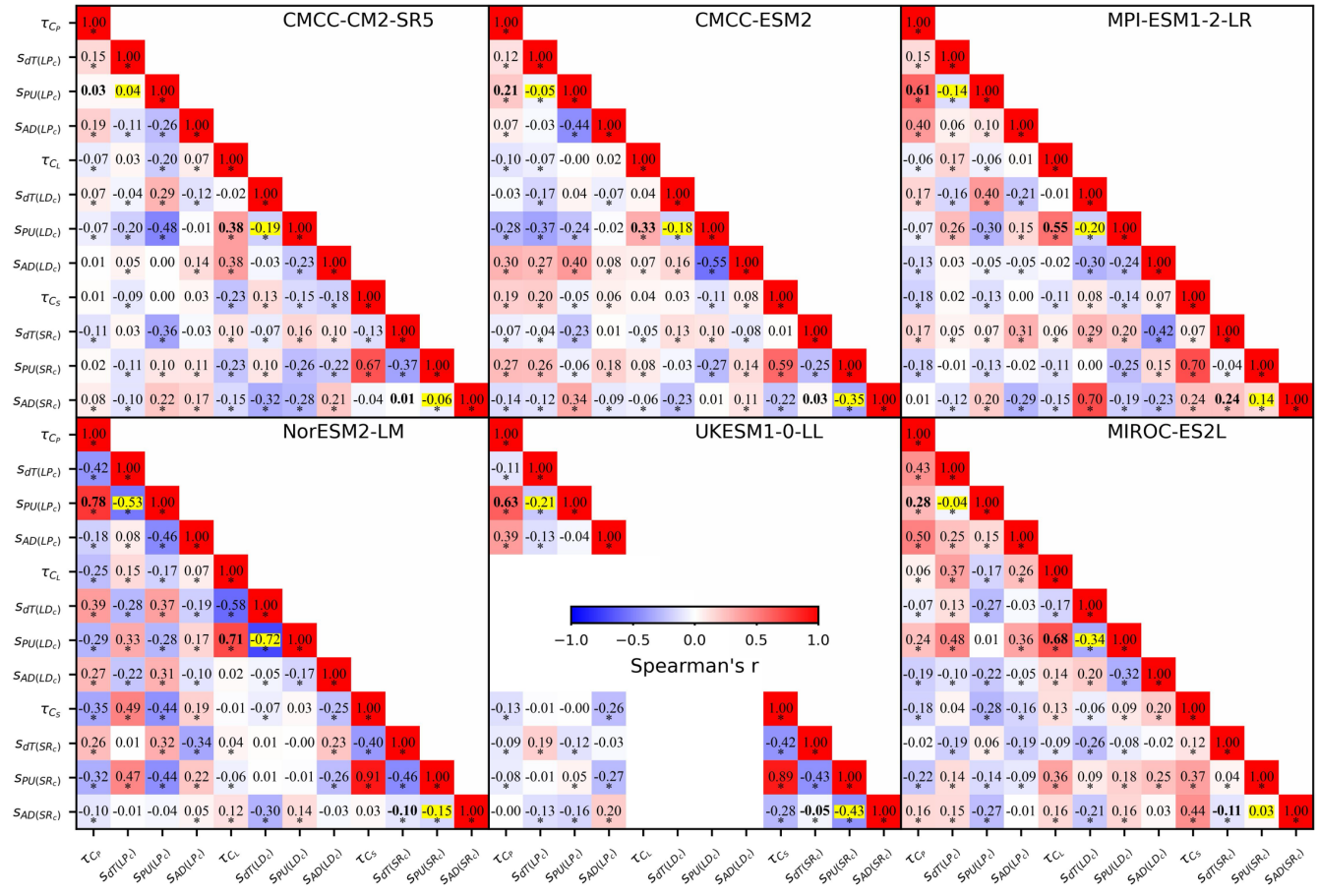

Figure A7. Correlation of turnover times and feedback-related parameters from the CMIP6 ESMs (numbers in the boxes refer to the Spearman's r between pairs of parameters; * indicates the p-value < 0.001; the correlations between temperature sensitivities and plant nitrogen uptake sensitivities are highlighted in yellow; the correlations between turnover times and plant nitrogen uptake sensitivities are displayed in bold font).

https://doi.org/10.5194/egusphere-2024-1941
Preprint. Discussion started: 18 September 2024

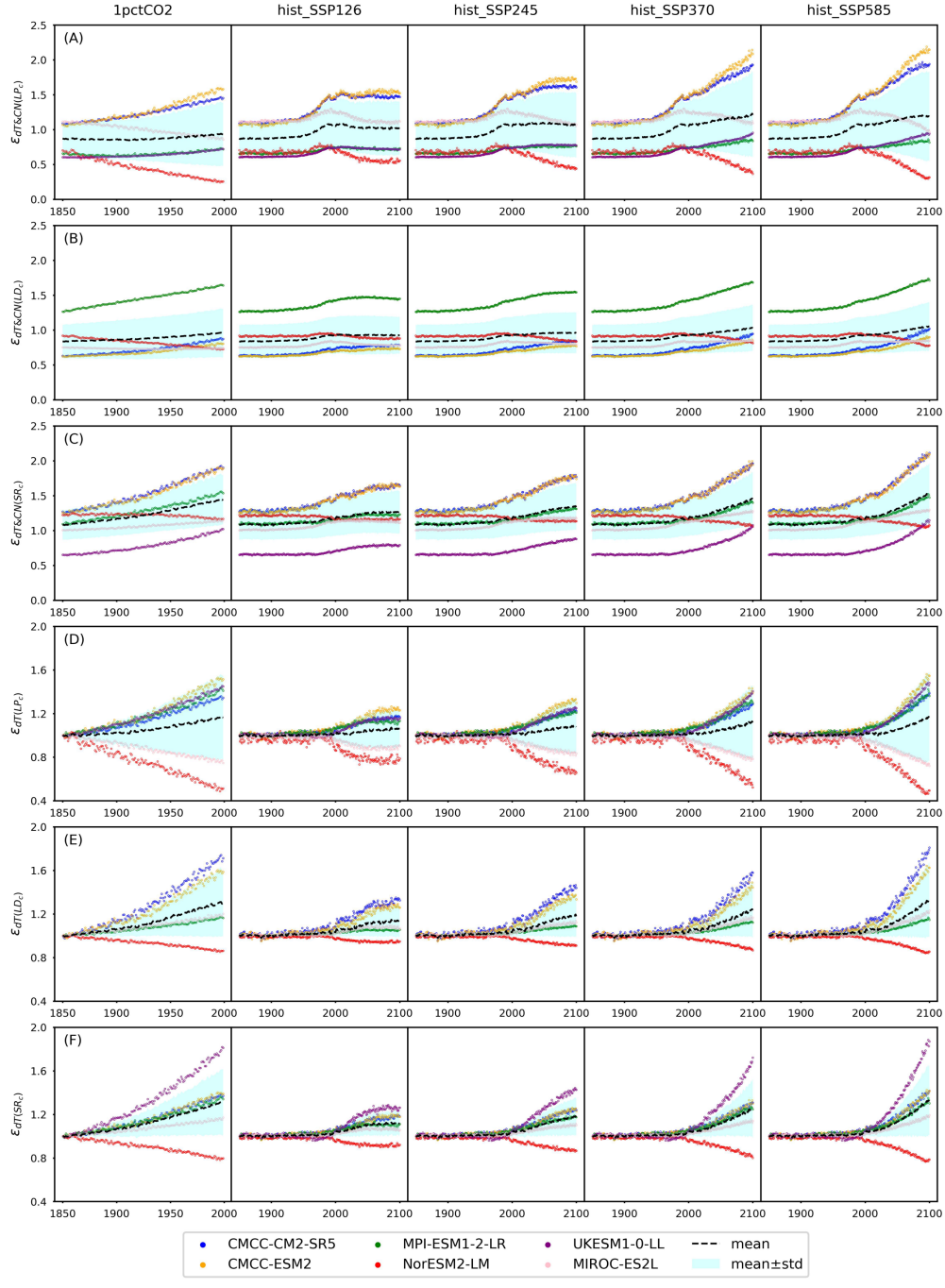

Figure A8. The emulated overall and temperature effect on carbon pool turnovers, including litter production ($\epsilon_{dT\&CN(LP_c)}$ and $\epsilon_{dT(LP_c)}$, litter decomposition ($\epsilon_{dT\&CN(LD_c)}$ and $\epsilon_{dT(LD_c)}$), and soil respiration ($\epsilon_{dT\&CN(SR_c)}$ and $\epsilon_{dT(SR_c)}$) from CMIP6 ESMs across different scenarios.

https://doi.org/10.5194/egusphere-2024-1941
Preprint. Discussion started: 18 September 2024

Code and data availability

The model code is available at https://doi.org/10.5281/zenodo.12204422 (Tang et al., 2024). The calibration data is accessible either from the original publications (for CABLE and OCN) or through the Earth System Grid Federation (ESGF, for CMIP6 ESM output), with details provided in Section 3.1 Data Acquisition and Processing.

Author contribution

GT and MM conceptualized the idea of carbon-nitrogen coupling in MAGICC. GT designed, coded, and calibrated the coupled carbon-nitrogen model. ZN, AN, SZ, and MM contributed to the model improvement. ZN assisted with code implementation and optimization. SZ provided the OCN dataset used for model calibration. ZN, SZ, and MM were responsible for funding acquisition. GT analyzed and interpreted the results and wrote the first draft of the manuscript. All authors contributed to writing and revising the manuscript.

Competing interests

The authors declare that they have no conflict of interest.

Acknowledgements

This work is supported by the Australian National Environmental Science Program (Climate Systems Hub, Malte Meinshausen) and the European Union's Horizon 2020 Research and Innovation Funding Programme (No. 101003536, Earth System Models for the Future, ESM2025, Zebedee Nicholls and Sönke Zaehle).

We express our sincere gratitude to Dr. Peter Rayner from the Superpower Institute and The University of Melbourne, Dr. Chris Jones and Dr. Andrew Wiltshire from the Met Office Hadley Centre, Dr. Ying-Ping Wang and Dr. Tilo Ziehn from the Commonwealth Scientific and Industrial Research Organisation, Dr. Cheng Gong and Dr. Katrin Fleischer from the Max Planck Institute for Biogeochemistry, Dr. Trevor Sloughter and Dr. Bonnie Waring from Imperial College London, and others for their valuable contributions through insightful discussions, collaborations, data sharing, and continuous support. Additionally, we extend our thanks to World Climate Research Programme (WCRP), Coupled Model Intercomparison Project Phase 6 (CMIP6), Coupled Climate-Carbon Cycle Model Intercomparison Project (C4MIP), Earth System Grid Federation (ESGF), and the Earth system model (ESM) groups for their collective efforts in making the ESM output available and accessible.

https://doi.org/10.5194/egusphere-2024-1941
Preprint. Discussion started: 18 September 2024

References

Alvarez-Clare, S., Mack, M. C., and Brooks, M.: A direct test of nitrogen and phosphorus limitation to net primary productivity in a lowland tropical wet forest, Ecology, 94, 1540-1551, https://doi.org/10.1890/12-2128.1, 2013.

Anav, A., Friedlingstein, P., Kidston, M., Bopp, L., Ciais, P., Cox, P., Jones, C., Jung, M., Myneni, R., and Zhu, Z.: Evaluating the Land and Ocean Components of the Global Carbon Cycle in the CMIP5 Earth System Models, Journal of Climate, 26, 6801-6843, https://doi.org/10.1175/JCLI-D-12-00417.1, 2013.

Arora, V. K., Katavouta, A., Williams, R. G., Jones, C. D., Brovkin, V., Friedlingstein, P., Schwinger, J., Bopp, L., Boucher, O., Cadule, P., Chamberlain, M. A., Christian, J. R., Delire, C., Fisher, R. A., Hajima, T., Ilyina, T., Joetzjer, E., Kawamiya, M., Koven, C. D., Krasting, J. P., Law, R. M., Lawrence, D. M., Lenton, A., Lindsay, K., Pongratz, J., Raddatz, T., Séférian, R., Tachiiri, K., Tjiputra, J. F., Wiltshire, A., Wu, T., and Ziehn, T.: Carbon–concentration and carbon–climate feedbacks in CMIP6 models and their comparison to CMIP5 models, Biogeosciences, 17, 4173-4222, 10.5194/bg-17-4173-2020, 2020.

Averill, C. and Waring, B.: Nitrogen limitation of decomposition and decay: How can it occur?, Global Change Biology, 24, 1417-1427, https://doi.org/10.1111/gcb.13980, 2018.

Bacastow, R. and Keeling, C. D.: Atmospheric carbon dioxide and radiocarbon in the natural carbon cycle: II. Changes from AD 1700 to 2070 as deduced from a geochemical model, Brookhaven Symposia in Biology, 86-135,

Bardgett, R. D., Mawdsley, J. L., Edwards, S., Hobbs, P. J., Rodwell, J. S., and Davies, W. J.: Plant species and nitrogen effects on soil biological properties of temperate upland grasslands, Functional Ecology, 13, 650-660, https://doi.org/10.1046/j.1365-2435.1999.00362.x, 1999.

Bi, D., Dix, M., Marsland, S., O'Farrell, S., Sullivan, A., Bodman, R., Law, R., Harman, I., Srbinovsky, J., Rashid, H. A., Dobrohotoff, P., Mackallah, C., Yan, H., Hirst, A., Savita, A., Dias, F. B., Woodhouse, M., Fiedler, R., and Heerdegen, A.: Configuration and spin-up of ACCESS-CM2, the new generation Australian Community Climate and Earth System Simulator Coupled Model, Journal of Southern Hemisphere Earth Systems Science, 70, 225-251, https://doi.org/10.1071/ES19040, 2020.

Bodman, R. W., Rayner, P. J., and Karoly, D. J.: Uncertainty in temperature projections reduced using carbon cycle and climate observations, Nature Climate Change, 3, 725-729, 10.1038/nclimate1903, 2013.

Boucher, O., Servonnat, J., Albright, A. L., Aumont, O., Balkanski, Y., Bastrikov, V., Bekki, S., Bonnet, R., Bony, S., Bopp, L., Braconnot, P., Brockmann, P., Cadule, P., Caubel, A., Cheruy, F., Codron, F., Cozic, A., Cugnet, D., D'Andrea, F., Davini, P., de Lavergne, C., Denvil, S., Deshayes, J., Devilliers, M., Ducharne, A., Dufresne, J.-L., Dupont, E., Éthé, C., Fairhead, L., Falletti, L., Flavoni, S., Foujols, M.-A., Gardoll, S., Gastineau, G., Ghattas, J., Grandpeix, J.-Y., Guenet, B., Guez, L., E., Guilyardi, E., Guimberteau, M., Hauglustaine, D., Hourdin, F., Idelkadi, A., Joussaume, S., Kageyama, M., Khodri, M., Krinner, G., Lebas, N., Levavasseur, G., Lévy, C., Li, L., Lott, F., Lurton, T., Luyssaert, S., Madec, G., Madeleine, J.-B., Maignan, F., Marchand, M., Marti, O., Mellul, L., Meurdesoif, Y., Mignot, J., Musat, I., Ottlé, C., Peylin, P., Planton, Y., Polcher, J., Rio, C., Rochetin, N., Rousset, C., Sepulchre, P., Sima, A., Swingedouw, D., Thiéblemont, R.,

Traore, A. K., Vancoppenolle, M., Vial, J., Vialard, J., Viovy, N., and Vuichard, N.: Presentation and Evaluation of the IPSL-CM6A-LR Climate Model, Journal of Advances in Modeling Earth Systems, 12, e2019MS002010, https://doi.org/10.1029/2019MS002010, 2020.

Cherchi, A., Fogli, P. G., Lovato, T., Peano, D., Iovino, D., Gualdi, S., Masina, S., Scoccimarro, E., Materia, S., Bellucci, A., and Navarra, A.: Global Mean Climate and Main Patterns of Variability in the CMCC-CM2 Coupled Model, Journal of Advances in Modeling Earth Systems, 11, 185-209, https://doi.org/10.1029/2018MS001369, 2019.

Ciais, P., Sabine, C., Bala, G., Bopp, L., Brovkin, V., Canadell, J., Chhabra, A., DeFries, R., Galloway, J., and Heimann, M.: Carbon and other biogeochemical cycles, in: Climate change 2013: the physical science basis. Contribution of Working Group I to the Fifth Assessment Report of the Intergovernmental Panel on Climate Change, Cambridge University Press, 465-570, 2014.

Cleveland, C. C., Townsend, A. R., Schimel, D. S., Fisher, H., Howarth, R. W., Hedin, L. O., Perakis, S. S., Latty, E. F., Von Fischer, J. C., Elseroad, A., and Wasson, M. F.: Global patterns of terrestrial biological nitrogen (N2) fixation in natural ecosystems, Global Biogeochemical Cycles, 13, 623-645, https://doi.org/10.1029/1999GB900014, 1999.

Collier, N., Hoffman, F. M., Lawrence, D. M., Keppel-Aleks, G., Koven, C. D., Riley, W. J., Mu, M., and Randerson, J. T.: The International Land Model Benchmarking (ILAMB) System: Design, Theory, and Implementation, Journal of Advances in Modeling Earth Systems, 10, 2731-2754, https://doi.org/10.1029/2018MS001354, 2018.

Craine, J. M., Morrow, C., and Fierer, N.: MICROBIAL NITROGEN LIMITATION INCREASES DECOMPOSITION, Ecology, 88, 2105-2113, https://doi.org/10.1890/06-1847.1, 2007.

Cusack, D. F., Silver, W. L., Torn, M. S., and McDowell, W. H.: Effects of nitrogen additions on above- and belowground carbon dynamics in two tropical forests, Biogeochemistry, 104, 203-225, 10.1007/s10533-010-9496-4, 2011.

Cusack, D. F., Torn, M. S., McDowell, W. H., and Silver, W. L.: The response of heterotrophic activity and carbon cycling to nitrogen additions and warming in two tropical soils, Global Change Biology, 16, 2555-2572, https://doi.org/10.1111/j.1365-2486.2009.02131.x, 2010.

Davies-Barnard, T. and Friedlingstein, P.: The Global Distribution of Biological Nitrogen Fixation in Terrestrial Natural Ecosystems, Global Biogeochemical Cycles, 34, e2019GB006387, https://doi.org/10.1029/2019GB006387, 2020.

Davies-Barnard, T., Zaehle, S., and Friedlingstein, P.: Assessment of the impacts of biological nitrogen fixation structural uncertainty in CMIP6 earth system models, Biogeosciences, 19, 3491-3503, 10.5194/bg-19-3491-2022, 2022.

Davies-Barnard, T., Meyerholt, J., Zaehle, S., Friedlingstein, P., Brovkin, V., Fan, Y., Fisher, R. A., Jones, C. D., Lee, H., Peano, D., Smith, B., Wårlind, D., and Wiltshire, A. J.: Nitrogen cycling in CMIP6 land surface models: progress and limitations, Biogeosciences, 17, 5129-5148, 10.5194/bg-17-5129-2020, 2020.

Deser, C., Phillips, A., Bourdette, V., and Teng, H.: Uncertainty in climate change projections: the role of internal variability, Climate dynamics, 38, 527-546, 2012.

Deser, C., Lehner, F., Rodgers, K. B., Ault, T., Delworth, T. L., DiNezio, P. N., Fiore, A., Frankignoul, C., Fyfe, J. C., Horton, D. E., Kay, J. E., Knutti, R., Lovenduski, N. S., Marotzke, J., McKinnon, K. A., Minobe, S., Randerson, J., Screen,

https://doi.org/10.5194/egusphere-2024-1941
Preprint. Discussion started: 18 September 2024

J. A., Simpson, I. R., and Ting, M.: Insights from Earth system model initial-condition large ensembles and future prospects, Nature Climate Change, 10, 277-286, 10.1038/s41558-020-0731-2, 2020.

Du, Z., Weng, E., Jiang, L., Luo, Y., Xia, J., and Zhou, X.: Carbon–nitrogen coupling under three schemes of model representation: a traceability analysis, Geosci. Model Dev., 11, 4399-4416, 10.5194/gmd-11-4399-2018, 2018.

Duan, Y., Kumar, S., and Kinter, J. L.: Evaluation of Long-Term Temperature Trend and Variability in CMIP6 Multimodel Ensemble, Geophysical Research Letters, 48, e2021GL093227, https://doi.org/10.1029/2021GL093227, 2021.

Elser, J. J., Bracken, M. E. S., Cleland, E. E., Gruner, D. S., Harpole, W. S., Hillebrand, H., Ngai, J. T., Seabloom, E. W., Shurin, J. B., and Smith, J. E.: Global analysis of nitrogen and phosphorus limitation of primary producers in freshwater, marine and terrestrial ecosystems, Ecology Letters, 10, 1135-1142, https://doi.org/10.1111/j.1461-0248.2007.01113.x, 2007.

Eyring, V., Bony, S., Meehl, G. A., Senior, C. A., Stevens, B., Stouffer, R. J., and Taylor, K. E.: Overview of the Coupled Model Intercomparison Project Phase 6 (CMIP6) experimental design and organization, Geosci. Model Dev., 9, 1937-1958, 10.5194/gmd-9-1937-2016, 2016.

Eyring, V., Cox, P. M., Flato, G. M., Gleckler, P. J., Abramowitz, G., Caldwell, P., Collins, W. D., Gier, B. K., Hall, A. D., Hoffman, F. M., Hurtt, G. C., Jahn, A., Jones, C. D., Klein, S. A., Krasting, J. P., Kwiatkowski, L., Lorenz, R., Maloney, E., Meehl, G. A., Pendergrass, A. G., Pincus, R., Ruane, A. C., Russell, J. L., Sanderson, B. M., Santer, B. D., Sherwood, S. C., Simpson, I. R., Stouffer, R. J., and Williamson, M. S.: Taking climate model evaluation to the next level, Nature Climate Change, 9, 102-110, 10.1038/s41558-018-0355-y, 2019.

Fan, X., Duan, Q., Shen, C., Wu, Y., and Xing, C.: Global surface air temperatures in CMIP6: historical performance and future changes, Environmental Research Letters, 15, 104056, 2020.

Flato, G., Marotzke, J., Abiodun, B., Braconnot, P., Chou, S. C., Collins, W., Cox, P., Driouech, F., Emori, S., and Eyring, V.: Evaluation of climate models, in: Climate change 2013: the physical science basis. Contribution of Working Group I to the Fifth Assessment Report of the Intergovernmental Panel on Climate Change, Cambridge University Press, 741-866, 2014.

Fleischer, K., Dolman, A. J., van der Molen, M. K., Rebel, K. T., Erisman, J. W., Wassen, M. J., Pak, B., Lu, X., Rammig, A., and Wang, Y.-P.: Nitrogen Deposition Maintains a Positive Effect on Terrestrial Carbon Sequestration in the 21st Century Despite Growing Phosphorus Limitation at Regional Scales, Global Biogeochemical Cycles, 33, 810-824, https://doi.org/10.1029/2018GB005952, 2019.

Forsmark, B., Nordin, A., Maaroufi, N. I., Lundmark, T., and Gundale, M. J.: Low and High Nitrogen Deposition Rates in Northern Coniferous Forests Have Different Impacts on Aboveground Litter Production, Soil Respiration, and Soil Carbon Stocks, Ecosystems, 23, 1423-1436, 10.1007/s10021-020-00478-8, 2020.

Fowler, D., Coyle, M., Skiba, U., Sutton, M. A., Cape, J. N., Reis, S., Sheppard, L. J., Jenkins, A., Grizzetti, B., Galloway, J. N., Vitousek, P., Leach, A., Bouwman, A. F., Butterbach-Bahl, K., Dentener, F., Stevenson, D., Amann, M., and Voss, M.: The global nitrogen cycle in the twenty-first century, Philosophical Transactions of the Royal Society B: Biological Sciences, 368, 20130164, doi:10.1098/rstb.2013.0164, 2013.

https://doi.org/10.5194/egusphere-2024-1941
Preprint. Discussion started: 18 September 2024

Friedlingstein, P., Meinshausen, M., Arora, V. K., Jones, C. D., Anav, A., Liddicoat, S. K., and Knutti, R.: Uncertainties in CMIP5 Climate Projections due to Carbon Cycle Feedbacks, Journal of Climate, 27, 511-526, https://doi.org/10.1175/JCLI-D-12-00579.1, 2014.

Gao, F. and Han, L.: Implementing the Nelder-Mead simplex algorithm with adaptive parameters, Computational Optimization and Applications, 51, 259-277, 10.1007/s10589-010-9329-3, 2012.

Gasser, T. and Ciais, P.: A theoretical framework for the net land-to-atmosphere CO₂ flux and its implications in the definition of "emissions from land-use change", Earth Syst. Dynam., 4, 171-186, 10.5194/esd-4-171-2013, 2013.

Gifford, R. M.: Implications of CO_2 Effects on Vegetation for the Global Carbon Budget, The Global Carbon Cycle, Berlin, Heidelberg, 1993//, 159-199,

Goll, D. S., Winkler, A. J., Raddatz, T., Dong, N., Prentice, I. C., Ciais, P., and Brovkin, V.: Carbon–nitrogen interactions in idealized simulations with JSBACH (version 3.10), Geosci. Model Dev., 10, 2009-2030, 10.5194/gmd-10-2009-2017, 2017.

Gruber, N. and Galloway, J. N.: An Earth-system perspective of the global nitrogen cycle, Nature, 451, 293-296, 10.1038/nature06592, 2008.

Hajima, T., Watanabe, M., Yamamoto, A., Tatebe, H., Noguchi, M. A., Abe, M., Ohgaito, R., Ito, A., Yamazaki, D., Okajima, H., Ito, A., Takata, K., Ogochi, K., Watanabe, S., and Kawamiya, M.: Development of the MIROC-ES2L Earth system model and the evaluation of biogeochemical processes and feedbacks, Geosci. Model Dev., 13, 2197-2244, 10.5194/gmd-13-2197-2020, 2020.

Hedin, L. O., Brookshire, E. N. J., Menge, D. N. L., and Barron, A. R.: The Nitrogen Paradox in Tropical Forest Ecosystems, Annual Review of Ecology, Evolution, and Systematics, 40, 613-635, 10.1146/annurev.ecolsys.37.091305.110246, 2005.

Hobbie, S. E.: NITROGEN EFFECTS ON DECOMPOSITION: A FIVE-YEAR EXPERIMENT IN EIGHT TEMPERATE SITES, Ecology, 89, 2633-2644, https://doi.org/10.1890/07-1119.1, 2008.

Hunt, R., Hand, D. W., Hannah, M. A., and Neal, A. M.: Response to CO₂ Enrichment in 27 Herbaceous Species, Functional Ecology, 5, 410-421, 10.2307/2389813, 1991.

Jones, C. D., Arora, V., Friedlingstein, P., Bopp, L., Brovkin, V., Dunne, J., Graven, H., Hoffman, F., Ilyina, T., John, J. G., Jung, M., Kawamiya, M., Koven, C., Pongratz, J., Raddatz, T., Randerson, J. T., and Zaehle, S.: C4MIP – The Coupled Climate–Carbon Cycle Model Intercomparison Project: experimental protocol for CMIP6, Geosci. Model Dev., 9, 2853-2880, 10.5194/gmd-9-2853-2016, 2016.

Kou-Giesbrecht, S. and Arora, V. K.: Representing the Dynamic Response of Vegetation to Nitrogen Limitation via Biological Nitrogen Fixation in the CLASSIC Land Model, Global Biogeochemical Cycles, 36, e2022GB007341, https://doi.org/10.1029/2022GB007341, 2022.

Kumar, D. and Ganguly, A. R.: Intercomparison of model response and internal variability across climate model ensembles, Climate dynamics, 51, 207-219, 2018.

https://doi.org/10.5194/egusphere-2024-1941
Preprint. Discussion started: 18 September 2024

Kumar, S., Merwade, V., Kinter, J. L., and Niyogi, D.: Evaluation of Temperature and Precipitation Trends and Long-Term Persistence in CMIP5 Twentieth-Century Climate Simulations, Journal of Climate, 26, 4168-4185, https://doi.org/10.1175/JCLI-D-12-00259.1, 2013.

Law, R. M., Ziehn, T., Matear, R. J., Lenton, A., Chamberlain, M. A., Stevens, L. E., Wang, Y. P., Srbinovsky, J., Bi, D., Yan, H., and Vohralik, P. F.: The carbon cycle in the Australian Community Climate and Earth System Simulator (ACCESS-ESM1) – Part 1: Model description and pre-industrial simulation, Geosci. Model Dev., 10, 2567-2590, 10.5194/gmd-10-2567-2017, 2017.

Lawrence, D. M., Fisher, R. A., Koven, C. D., Oleson, K. W., Swenson, S. C., Bonan, G., Collier, N., Ghimire, B., van Kampenhout, L., Kennedy, D., Kluzek, E., Lawrence, P. J., Li, F., Li, H., Lombardozzi, D., Riley, W. J., Sacks, W. J., Shi, M., Vertenstein, M., Wieder, W. R., Xu, C., Ali, A. A., Badger, A. M., Bisht, G., van den Broeke, M., Brunke, M. A., Burns, S. P., Buzan, J., Clark, M., Craig, A., Dahlin, K., Drewniak, B., Fisher, J. B., Flanner, M., Fox, A. M., Gentine, P., Hoffman, F., Keppel-Aleks, G., Knox, R., Kumar, S., Lenaerts, J., Leung, L. R., Lipscomb, W. H., Lu, Y., Pandey, A., Pelletier, J. D., Perket, J., Randerson, J. T., Ricciuto, D. M., Sanderson, B. M., Slater, A., Subin, Z. M., Tang, J., Thomas, R. Q., Val Martin, M., and Zeng, X.: The Community Land Model Version 5: Description of New Features, Benchmarking, and Impact of Forcing Uncertainty, Journal of Advances in Modeling Earth Systems, 11, 4245-4287, https://doi.org/10.1029/2018MS001583, 2019.

LeBauer, D. S. and Treseder, K. K.: NITROGEN LIMITATION OF NET PRIMARY PRODUCTIVITY IN TERRESTRIAL ECOSYSTEMS IS GLOBALLY DISTRIBUTED, Ecology, 89, 371-379, 10.1890/06-2057.1, 2008.

Li, Z., Tian, D., Wang, B., Wang, J., Wang, S., Chen, H. Y. H., Xu, X., Wang, C., He, N., and Niu, S.: Microbes drive global soil nitrogen mineralization and availability, Global Change Biology, 25, 1078-1088, https://doi.org/10.1111/gcb.14557, 2019.

Lim, H., Oren, R., Palmroth, S., Tor-ngern, P., Mörling, T., Näsholm, T., Lundmark, T., Helmisaari, H.-S., Leppälammi-Kujansuu, J., and Linder, S.: Inter-annual variability of precipitation constrains the production response of boreal Pinus sylvestris to nitrogen fertilization, Forest Ecology and Management, 348, 31-45, https://doi.org/10.1016/j.foreco.2015.03.029, 2015.

Lovato, T., Peano, D., Butenschön, M., Materia, S., Iovino, D., Scoccimarro, E., Fogli, P. G., Cherchi, A., Bellucci, A., Gualdi, S., Masina, S., and Navarra, A.: CMIP6 Simulations With the CMCC Earth System Model (CMCC-ESM2), Journal of Advances in Modeling Earth Systems, 14, e2021MS002814, https://doi.org/10.1029/2021MS002814, 2022.

Lovenduski, N. S. and Bonan, G. B.: Reducing uncertainty in projections of terrestrial carbon uptake, Environmental Research Letters, 12, 044020, 2017.

Manzoni, S., Jackson, R. B., Trofymow, J. A., and Porporato, A.: The Global Stoichiometry of Litter Nitrogen Mineralization, Science, 321, 684-686, doi:10.1126/science.1159792, 2008.

Mauritsen, T., Bader, J., Becker, T., Behrens, J., Bittner, M., Brokopf, R., Brovkin, V., Claussen, M., Crueger, T., Esch, M., Fast, I., Fiedler, S., Fläschner, D., Gayler, V., Giorgetta, M., Goll, D. S., Haak, H., Hagemann, S., Hedemann, C.,

https://doi.org/10.5194/egusphere-2024-1941
Preprint. Discussion started: 18 September 2024

Hohenegger, C., Ilyina, T., Jahns, T., Jimenéz-de-la-Cuesta, D., Jungclaus, J., Kleinen, T., Kloster, S., Kracher, D., Kinne, S., Kleberg, D., Lasslop, G., Kornblueh, L., Marotzke, J., Matei, D., Meraner, K., Mikolajewicz, U., Modali, K., Möbis, B., Müller, W. A., Nabel, J. E. M. S., Nam, C. C. W., Notz, D., Nyawira, S.-S., Paulsen, H., Peters, K., Pincus, R., Pohlmann, H., Pongratz, J., Popp, M., Raddatz, T. J., Rast, S., Redler, R., Reick, C. H., Rohrschneider, T., Schemann, V., Schmidt, H., Schnur, R., Schulzweida, U., Six, K. D., Stein, L., Stemmler, I., Stevens, B., von Storch, J.-S., Tian, F., Voigt, A., Vrese, P., Wieners, K.-H., Wilkenskjeld, S., Winkler, A., and Roeckner, E.: Developments in the MPI-M Earth System Model version 1.2 (MPI-ESM1.2) and Its Response to Increasing CO2, Journal of Advances in Modeling Earth Systems, 11, 998-1038, https://doi.org/10.1029/2018MS001400, 2019.

Meehl, G. A.: Development of global coupled ocean-atmosphere general circulation models, Climate Dynamics, 5, 19-33, 10.1007/BF00195851, 1990.

Meehl, G. A., Senior, C. A., Eyring, V., Flato, G., Lamarque, J.-F., Stouffer, R. J., Taylor, K. E., and Schlund, M.: Context for interpreting equilibrium climate sensitivity and transient climate response from the CMIP6 Earth system models, Science Advances, 6, eaba1981, doi:10.1126/sciadv.aba1981, 2020.

Meinshausen, M., Raper, S. C. B., and Wigley, T. M. L.: Emulating coupled atmosphere-ocean and carbon cycle models with a simpler model, MAGICC6 – Part 1: Model description and calibration, Atmos. Chem. Phys., 11, 1417-1456, 10.5194/acp-11-1417-2011, 2011a.

Meinshausen, M., Smith, S. J., Calvin, K., Daniel, J. S., Kainuma, M. L. T., Lamarque, J. F., Matsumoto, K., Montzka, S. A., Raper, S. C. B., Riahi, K., Thomson, A., Velders, G. J. M., and van Vuuren, D. P. P.: The RCP greenhouse gas concentrations and their extensions from 1765 to 2300, Climatic Change, 109, 213, 10.1007/s10584-011-0156-z, 2011b.

Meinshausen, M., Nicholls, Z. R. J., Lewis, J., Gidden, M. J., Vogel, E., Freund, M., Beyerle, U., Gessner, C., Nauels, A., Bauer, N., Canadell, J. G., Daniel, J. S., John, A., Krummel, P. B., Luderer, G., Meinshausen, N., Montzka, S. A., Rayner, P. J., Reimann, S., Smith, S. J., van den Berg, M., Velders, G. J. M., Vollmer, M. K., and Wang, R. H. J.: The shared socio-economic pathway (SSP) greenhouse gas concentrations and their extensions to 2500, Geosci. Model Dev., 13, 3571-3605, 10.5194/gmd-13-3571-2020, 2020.

Meinshausen, M., Vogel, E., Nauels, A., Lorbacher, K., Meinshausen, N., Etheridge, D. M., Fraser, P. J., Montzka, S. A., Rayner, P. J., Trudinger, C. M., Krummel, P. B., Beyerle, U., Canadell, J. G., Daniel, J. S., Enting, I. G., Law, R. M., Lunder, C. R., O'Doherty, S., Prinn, R. G., Reimann, S., Rubino, M., Velders, G. J. M., Vollmer, M. K., Wang, R. H. J., and Weiss, R.: Historical greenhouse gas concentrations for climate modelling (CMIP6), Geosci. Model Dev., 10, 2057-2116, 10.5194/gmd-10-2057-2017, 2017.

Melnikova, I., Boucher, O., Cadule, P., Ciais, P., Gasser, T., Quilcaille, Y., Shiogama, H., Tachiiri, K., Yokohata, T., and Tanaka, K.: Carbon Cycle Response to Temperature Overshoot Beyond 2°C: An Analysis of CMIP6 Models, Earth's Future, 9, e2020EF001967, https://doi.org/10.1029/2020EF001967, 2021.

Menge, D. N. L., Hedin, L. O., and Pacala, S. W.: Nitrogen and Phosphorus Limitation over Long-Term Ecosystem Development in Terrestrial Ecosystems, PLOS ONE, 7, e42045, 10.1371/journal.pone.0042045, 2012.

https://doi.org/10.5194/egusphere-2024-1941
Preprint. Discussion started: 18 September 2024

Meyerholt, J. and Zaehle, S.: The role of stoichiometric flexibility in modelling forest ecosystem responses to nitrogen fertilization, New Phytologist, 208, 1042-1055, https://doi.org/10.1111/nph.13547, 2015.

Meyerholt, J., Sickel, K., and Zaehle, S.: Ensemble projections elucidate effects of uncertainty in terrestrial nitrogen limitation on future carbon uptake, Global Change Biology, 26, 3978-3996, https://doi.org/10.1111/gcb.15114, 2020.

Meyerholt, J., Zaehle, S., and Smith, M. J.: Variability of projected terrestrial biosphere responses to elevated levels of atmospheric CO_2 due to uncertainty in biological nitrogen fixation, Biogeosciences, 13, 1491-1518, 10.5194/bg-13-1491-2016, 2016.

Mulvaney, R. L., Khan, S. A., and Ellsworth, T. R.: Synthetic Nitrogen Fertilizers Deplete Soil Nitrogen: A Global Dilemma for Sustainable Cereal Production, Journal of Environmental Quality, 38, 2295-2314, https://doi.org/10.2134/jeq2008.0527, 2009.

Nauels, A., Meinshausen, M., Mengel, M., Lorbacher, K., and Wigley, T. M. L.: Synthesizing long-term sea level rise projections – the MAGICC sea level model v2.0, Geosci. Model Dev., 10, 2495-2524, 10.5194/gmd-10-2495-2017, 2017.

Nicholls, Z., Meinshausen, M., Lewis, J., Corradi, M. R., Dorheim, K., Gasser, T., Gieseke, R., Hope, A. P., Leach, N. J., McBride, L. A., Quilcaille, Y., Rogelj, J., Salawitch, R. J., Samset, B. H., Sandstad, M., Shiklomanov, A., Skeie, R. B., Smith, C. J., Smith, S. J., Su, X., Tsutsui, J., Vega-Westhoff, B., and Woodard, D. L.: Reduced Complexity Model Intercomparison Project Phase 2: Synthesizing Earth System Knowledge for Probabilistic Climate Projections, Earth's Future, 9, e2020EF001900, 10.1029/2020EF001900, 2021.

Nicholls, Z. R. J., Meinshausen, M., Lewis, J., Gieseke, R., Dommenget, D., Dorheim, K., Fan, C. S., Fuglestvedt, J. S., Gasser, T., Golüke, U., Goodwin, P., Hartin, C., Hope, A. P., Kriegler, E., Leach, N. J., Marchegiani, D., McBride, L. A., Quilcaille, Y., Rogelj, J., Salawitch, R. J., Samset, B. H., Sandstad, M., Shiklomanov, A. N., Skeie, R. B., Smith, C. J., Smith, S., Tanaka, K., Tsutsui, J., and Xie, Z.: Reduced Complexity Model Intercomparison Project Phase 1: introduction and evaluation of global-mean temperature response, Geosci. Model Dev., 13, 5175-5190, 10.5194/gmd-13-5175-2020, 2020.

Ohgaito, R., Sueyoshi, T., Abe-Ouchi, A., Hajima, T., Watanabe, S., Kim, H. J., Yamamoto, A., and Kawamiya, M.: Can an Earth System Model simulate better climate change at mid-Holocene than an AOGCM? A comparison study of MIROC-ESM and MIROC3, Clim. Past, 9, 1519-1542, 10.5194/cp-9-1519-2013, 2013.

Papalexiou, S. M., Rajulapati, C. R., Clark, M. P., and Lehner, F.: Robustness of CMIP6 Historical Global Mean Temperature Simulations: Trends, Long-Term Persistence, Autocorrelation, and Distributional Shape, Earth's Future, 8, e2020EF001667, https://doi.org/10.1029/2020EF001667, 2020.

Phoenix, G. K., Hicks, W. K., Cinderby, S., Kuylenstierna, J. C. I., Stock, W. D., Dentener, F. J., Giller, K. E., Austin, A. T., Lefroy, R. D. B., Gimeno, B. S., Ashmore, M. R., and Ineson, P.: Atmospheric nitrogen deposition in world biodiversity hotspots: the need for a greater global perspective in assessing N deposition impacts, Global Change Biology, 12, 470-476, https://doi.org/10.1111/j.1365-2486.2006.01104.x, 2006.

https://doi.org/10.5194/egusphere-2024-1941
Preprint. Discussion started: 18 September 2024

Plett, D. C., Ranathunge, K., Melino, V. J., Kuya, N., Uga, Y., and Kronzucker, H. J.: The intersection of nitrogen nutrition and water use in plants: new paths toward improved crop productivity, Journal of Experimental Botany, 71, 4452-4468, 10.1093/jxb/eraa049, 2020.

Ramm, E., Liu, C., Ambus, P., Butterbach-Bahl, K., Hu, B., Martikainen, P. J., Marushchak, M. E., Mueller, C. W., Rennenberg, H., Schloter, M., Siljanen, H. M. P., Voigt, C., Werner, C., Biasi, C., and Dannenmann, M.: A review of the importance of mineral nitrogen cycling in the plant-soil-microbe system of permafrost-affected soils—changing the paradigm, Environmental Research Letters, 17, 013004, 10.1088/1748-9326/ac417e, 2022.

RANDERSON, J. T., HOFFMAN, F. M., THORNTON, P. E., MAHOWALD, N. M., LINDSAY, K., LEE, Y.-H., NEVISON, C. D., DONEY, S. C., BONAN, G., STÖCKLI, R., COVEY, C., RUNNING, S. W., and FUNG, I. Y.: Systematic assessment of terrestrial biogeochemistry in coupled climate–carbon models, Global Change Biology, 15, 2462-2484, https://doi.org/10.1111/j.1365-2486.2009.01912.x, 2009.

Reay, D. S., Dentener, F., Smith, P., Grace, J., and Feely, R. A.: Global nitrogen deposition and carbon sinks, Nature Geoscience, 1, 430-437, 10.1038/ngeo230, 2008.

Reich, P. B., Hobbie, S. E., and Lee, T. D.: Plant growth enhancement by elevated CO_2 eliminated by joint water and nitrogen limitation, Nature Geoscience, 7, 920-924, 10.1038/ngeo2284, 2014.

Rugenstein, M., Bloch-Johnson, J., Gregory, J., Andrews, T., Mauritsen, T., Li, C., Frölicher, T. L., Paynter, D., Danabasoglu, G., Yang, S., Dufresne, J.-L., Cao, L., Schmidt, G. A., Abe-Ouchi, A., Geoffroy, O., and Knutti, R.: Equilibrium Climate Sensitivity Estimated by Equilibrating Climate Models, Geophysical Research Letters, 47, e2019GL083898, https://doi.org/10.1029/2019GL083898, 2020.

Scafetta, N.: CMIP6 GCM ensemble members versus global surface temperatures, Climate Dynamics, 60, 3091-3120, 10.1007/s00382-022-06493-w, 2023.

Schulte-Uebbing, L. and de Vries, W.: Global-scale impacts of nitrogen deposition on tree carbon sequestration in tropical, temperate, and boreal forests: A meta-analysis, Global Change Biology, 24, e416-e431, https://doi.org/10.1111/gcb.13862, 2018.

Seland, Ø., Bentsen, M., Olivié, D., Toniazzo, T., Gjermundsen, A., Graff, L. S., Debernard, J. B., Gupta, A. K., He, Y. C., Kirkevåg, A., Schwinger, J., Tjiputra, J., Aas, K. S., Bethke, I., Fan, Y., Griesfeller, J., Grini, A., Guo, C., Ilicak, M., Karset, I. H. H., Landgren, O., Liakka, J., Moseid, K. O., Nummelin, A., Spensberger, C., Tang, H., Zhang, Z., Heinze, C., Iversen, T., and Schulz, M.: Overview of the Norwegian Earth System Model (NorESM2) and key climate response of CMIP6 DECK, historical, and scenario simulations, Geosci. Model Dev., 13, 6165-6200, 10.5194/gmd-13-6165-2020, 2020.

Sellar, A. A., Jones, C. G., Mulcahy, J. P., Tang, Y., Yool, A., Wiltshire, A., O'Connor, F. M., Stringer, M., Hill, R., Palmieri, J., Woodward, S., de Mora, L., Kuhlbrodt, T., Rumbold, S. T., Kelley, D. I., Ellis, R., Johnson, C. E., Walton, J., Abraham, N. L., Andrews, M. B., Andrews, T., Archibald, A. T., Berthou, S., Burke, E., Blockley, E., Carslaw, K., Dalvi, M., Edwards, J., Folberth, G. A., Gedney, N., Griffiths, P. T., Harper, A. B., Hendry, M. A., Hewitt, A. J., Johnson, B., Jones, A., Jones, C. D., Keeble, J., Liddicoat, S., Morgenstern, O., Parker, R. J., Predoi, V., Robertson, E., Siahaan, A.,

https://doi.org/10.5194/egusphere-2024-1941
Preprint. Discussion started: 18 September 2024

Smith, R. S., Swaminathan, R., Woodhouse, M. T., Zeng, G., and Zerroukat, M.: UKESM1: Description and Evaluation of the U.K. Earth System Model, Journal of Advances in Modeling Earth Systems, 11, 4513-4558, https://doi.org/10.1029/2019MS001739, 2019.

Sokolov, A. P., Kicklighter, D. W., Melillo, J. M., Felzer, B. S., Schlosser, C. A., and Cronin, T. W.: Consequences of Considering Carbon–Nitrogen Interactions on the Feedbacks between Climate and the Terrestrial Carbon Cycle, Journal of Climate, 21, 3776-3796, 10.1175/2008jcli2038.1, 2008.

Spafford, L. and MacDougall, A. H.: Validation of terrestrial biogeochemistry in CMIP6 Earth system models: a review, Geosci. Model Dev., 14, 5863-5889, 10.5194/gmd-14-5863-2021, 2021.

Stocker, B. D. and Joos, F.: Quantifying differences in land use emission estimates implied by definition discrepancies, Earth Syst. Dynam., 6, 731-744, 10.5194/esd-6-731-2015, 2015.

Storn, R. and Price, K.: Differential Evolution – A Simple and Efficient Heuristic for global Optimization over Continuous Spaces, Journal of Global Optimization, 11, 341-359, 10.1023/A:1008202821328, 1997.

Taylor, K. E., Stouffer, R. J., and Meehl, G. A.: An Overview of CMIP5 and the Experiment Design, Bulletin of the American Meteorological Society, 93, 485-498, https://doi.org/10.1175/BAMS-D-11-00094.1, 2012.

Tang, G., Nicholls, Z., Norton, A., Zaehle, S., and Meinshausen, M.: Model Source Code for "Coupled Carbon-Nitrogen Cycle in MAGICC: Model Description and Calibration". Zenodo. https://doi.org/10.5281/zenodo.12204422, 2024

Thomas, R. Q., Brookshire, E. N. J., and Gerber, S.: Nitrogen limitation on land: how can it occur in Earth system models?, Global Change Biology, 21, 1777-1793, https://doi.org/10.1111/gcb.12813, 2015.

Thomas, R. Q., Zaehle, S., Templer, P. H., and Goodale, C. L.: Global patterns of nitrogen limitation: confronting two global biogeochemical models with observations, Global Change Biology, 19, 2986-2998, https://doi.org/10.1111/gcb.12281, 2013.

Thornton, P. E., Lamarque, J.-F., Rosenbloom, N. A., and Mahowald, N. M.: Influence of carbon-nitrogen cycle coupling on land model response to CO_2 fertilization and climate variability, Global Biogeochemical Cycles, 21, 10.1029/2006GB002868, 2007.

Thornton, P. E., Doney, S. C., Lindsay, K., Moore, J. K., Mahowald, N., Randerson, J. T., Fung, I., Lamarque, J. F., Feddema, J. J., and Lee, Y. H.: Carbon-nitrogen interactions regulate climate-carbon cycle feedbacks: results from an atmosphere-ocean general circulation model, Biogeosciences, 6, 2099-2120, 10.5194/bg-6-2099-2009, 2009.

Varney, R. M., Chadburn, S. E., Burke, E. J., and Cox, P. M.: Evaluation of soil carbon simulation in CMIP6 Earth system models, Biogeosciences, 19, 4671-4704, 10.5194/bg-19-4671-2022, 2022.

Vitousek, P. M. and Howarth, R. W.: Nitrogen limitation on land and in the sea: How can it occur?, Biogeochemistry, 13, 87-115, 10.1007/BF00002772, 1991.

Vitousek, P. M., Cassman, K., Cleveland, C., Crews, T., Field, C. B., Grimm, N. B., Howarth, R. W., Marino, R., Martinelli, L., Rastetter, E. B., and Sprent, J. I.: Towards an ecological understanding of biological nitrogen fixation, in: The Nitrogen Cycle at Regional to Global Scales, edited by: Boyer, E. W., and Howarth, R. W., Springer Netherlands, Dordrecht, 1-45, 10.1007/978-94-017-3405-9_1, 2002.

https://doi.org/10.5194/egusphere-2024-1941
Preprint. Discussion started: 18 September 2024

Washington, W. M., Buja, L., and Craig, A.: The computational future for climate and Earth system models: on the path to petaflop and beyond, Philosophical Transactions of the Royal Society A: Mathematical, Physical and Engineering Sciences, 367, 833-846, doi:10.1098/rsta.2008.0219, 2009.

Wei, N., Xia, J., Zhou, J., Jiang, L., Cui, E., Ping, J., and Luo, Y.: Evolution of Uncertainty in Terrestrial Carbon Storage in Earth System Models from CMIP5 to CMIP6, Journal of Climate, 35, 5483-5499, https://doi.org/10.1175/JCLI-D-21-0763.1, 2022.

Wieder, W. R., Cleveland, C. C., Lawrence, D. M., and Bonan, G. B.: Effects of model structural uncertainty on carbon cycle projections: biological nitrogen fixation as a case study, Environmental Research Letters, 10, 044016, 10.1088/1748-9326/10/4/044016, 2015a.

Wieder, W. R., Cleveland, C. C., Smith, W. K., and Todd-Brown, K.: Future productivity and carbon storage limited by terrestrial nutrient availability, Nature Geoscience, 8, 441-444, 10.1038/ngeo2413, 2015b.

Wigley, T. M. L. and Raper, S. C. B.: Thermal expansion of sea water associated with global warming, Nature, 330, 127-131, 10.1038/330127a0, 1987.

Wigley, T. M. L. and Raper, S. C. B.: Implications for climate and sea level of revised IPCC emissions scenarios, Nature, 357, 293-300, 10.1038/357293a0, 1992.

Wigley, T. M. L. and Raper, S. C. B.: Interpretation of High Projections for Global-Mean Warming, Science, 293, 451-454, doi:10.1126/science.1061604, 2001.

Wiltshire, A. J., Burke, E. J., Chadburn, S. E., Jones, C. D., Cox, P. M., Davies-Barnard, T., Friedlingstein, P., Harper, A. B., Liddicoat, S., Sitch, S., and Zaehle, S.: JULES-CN: a coupled terrestrial carbon–nitrogen scheme (JULES vn5.1), Geosci. Model Dev., 14, 2161-2186, 10.5194/gmd-14-2161-2021, 2021.

Wright, S. J., Yavitt, J. B., Wurzburger, N., Turner, B. L., Tanner, E. V. J., Sayer, E. J., Santiago, L. S., Kaspari, M., Hedin, L. O., Harms, K. E., Garcia, M. N., and Corre, M. D.: Potassium, phosphorus, or nitrogen limit root allocation, tree growth, or litter production in a lowland tropical forest, Ecology, 92, 1616-1625, https://doi.org/10.1890/10-1558.1, 2011.

Zaehle, S.: Terrestrial nitrogen–carbon cycle interactions at the global scale, Philosophical Transactions of the Royal Society B: Biological Sciences, 368, 20130125, doi:10.1098/rstb.2013.0125, 2013.

Zaehle, S. and Dalmonech, D.: Carbon–nitrogen interactions on land at global scales: current understanding in modelling climate biosphere feedbacks, Current Opinion in Environmental Sustainability, 3, 311-320, 10.1016/j.cosust.2011.08.008, 2011.

Zaehle, S. and Friend, A. D.: Carbon and nitrogen cycle dynamics in the O-CN land surface model: 1. Model description, site-scale evaluation, and sensitivity to parameter estimates, Global Biogeochemical Cycles, 24, https://doi.org/10.1029/2009GB003521, 2010.

Zaehle, S., Friedlingstein, P., and Friend, A. D.: Terrestrial nitrogen feedbacks may accelerate future climate change, Geophysical Research Letters, 37, https://doi.org/10.1029/2009GL041345, 2010.

https://doi.org/10.5194/egusphere-2024-1941
Preprint. Discussion started: 18 September 2024

Zaehle, S., Jones, C. D., Houlton, B., Lamarque, J.-F., and Robertson, E.: Nitrogen Availability Reduces CMIP5 Projections of Twenty-First-Century Land Carbon Uptake, Journal of Climate, 28, 2494-2511, https://doi.org/10.1175/JCLI-D-13-00776.1, 2015.

Zaehle, S., Medlyn, B. E., De Kauwe, M. G., Walker, A. P., Dietze, M. C., Hickler, T., Luo, Y., Wang, Y.-P., El-Masri, B., Thornton, P., Jain, A., Wang, S., Warlind, D., Weng, E., Parton, W., Iversen, C. M., Gallet-Budynek, A., McCarthy, H., Finzi, A., Hanson, P. J., Prentice, I. C., Oren, R., and Norby, R. J.: Evaluation of 11 terrestrial carbon–nitrogen cycle models against observations from two temperate Free-Air CO_2 Enrichment studies, New Phytologist, 202, 803-822, 10.1111/nph.12697, 2014.

Zhu, Q., Castellano, M. J., and Yang, G.: Coupling soil water processes and the nitrogen cycle across spatial scales: Potentials, bottlenecks and solutions, Earth-Science Reviews, 187, 248-258, https://doi.org/10.1016/j.earscirev.2018.10.005, 2018.